END
DATE
FILMED
3 82
DTIC

1.0

4.5
5.0

2.8

2.5

3.2

2.2

1.1

36

40

2.0

1.8

1.25

1.4

1.6

MICROCOPY RESOLUTION TEST CHART

NATIONAL BUREAU OF STANDARDS 1963 A

REPORT DOCUMENTATION PAGE	READ INSTRUCTIONS BEFORE COMPLETING FORM

1. REPORT NUMBER NRL Memorandum Report 4726	2. GOVT ACCESSION NO. AD-A1J048	3. RECIPIENT'S CATALOG NUMBER

4. TITLE *(and Subtitle)* PRODUCTION OF INTENSE LIGHT ION BEAMS FROM A SUPERPOWER GENERATOR	5. TYPE OF REPORT & PERIOD COVERED Interim report on a continuing NRL problem.
	6. PERFORMING ORG. REPORT NUMBER

7. AUTHOR(s) F.C. Young, G. Cooperstein, S.A. Goldstein*, D. Mosher, S.J. Stephanakis, W.F. Oliphant, J.R. Boller, J. Maenchen¶, R.D. Genuario§, and R.N. Stringfield†	8. CONTRACT OR GRANT NUMBER(s)

9. PERFORMING ORGANIZATION NAME AND ADDRESS Naval Research Laboratory Washington, DC 20375	10. PROGRAM ELEMENT, PROJECT, TASK AREA & WORK UNIT NUMBERS 47-0875-01

11. CONTROLLING OFFICE NAME AND ADDRESS Defense Nuclear Agency Washington, DC 20305	12. REPORT DATE January 15, 1982
	13. NUMBER OF PAGES 56

14. MONITORING AGENCY NAME & ADDRESS(*if different from Controlling Office*)	15. SECURITY CLASS. *(of this report)* UNCLASSIFIED
	15a. DECLASSIFICATION/DOWNGRADING SCHEDULE

16. DISTRIBUTION STATEMENT *(of this Report)*

Approved for public release; distribution unlimited.

17. DISTRIBUTION STATEMENT *(of the abstract entered in Block 20, if different from Report)*

18. SUPPLEMENTARY NOTES

*Present address: JAYCOR, Inc., Alexandria, VA 22304.
¶Present address: Cornell University, Ithaca, NY 14850.
§Present address: Pulse Sciences, Inc., Oakland, CA 94612.
†Present address: Physics International Co., San Leandro, CA 94577.   (Continues)

19. KEY WORDS *(Continue on reverse side if necessary and identify by block number)*

Pulse power generators
Intense ion beams
Pinch-reflex diode
Ion beam focusing
Holographic interferometry

20. ABSTRACT *(Continue on reverse side if necessary and identify by block number)*

The operation of a pinch-reflex diode as an intense pulsed ion-beam source has been scaled up to the multiterawatt PITHON generator. Ion beams with currents of 1 MA at 1.8 MeV have been extracted in a 130 kJ, 100-ns (FWHM) pulse. The corresponding ion production efficiency is 60%. Power losses were observed in interfacing the coaxial diode to the biconic vacuum feed of the generator. By using smaller area diodes, the average current density at the anode source has been increased to 20 kA/cm^2. Proton and deuteron beams were studied in both planar and spherical diode geometries. The focusing of ion beams is predominately by self-magnetic fields for planar diodes and predominately by electrode

(Continues)

DD _{1 JAN 73} FORM 1473   EDITION OF 1 NOV 65 IS OBSOLETE
S/N 0102-014-6601

18. Supplementary Notes (Continued)

This research was sponsored by the Defense Nuclear Agency under DNA001-79-C-0023 and under DNA Subtask T99QAXLA014, work unit 46, and work unit title "Ion Beam Generation."

20. Abstract (Continued)

shaping for spherical diodes. Current densities of at least 150 kA/cm^2 were achieved with spherical diodes. The spatial evolution of the anode and cathode plasmas was studied by laser interferometric holography. As the peak of the power pulse is approached, plasmas were observed to expand from the electrodes in fairly uniform profiles with steep density gradients and to accelerate across the vacuum gap. After peak power, anode plasma fluctuations and a high velocity (30 cm/μs) axial plume develop; the latter expands radially coincident with collapse of the power pulse.

CONTENTS

Accession For

NTIS GRA&I ✓

DTIC TAB ☐

Unannounced ☐

Justification

By

Distribution/

Availability Codes

Ava'l and/or

Dist | Special

A

DTIC
SELECTED
FEB 3 1982
B

DTIC
COPY
INSPECTED
2

PREFACE

The purpose of the research effort described in this report was to investigate the scaling of the pinch-reflex ion diode, developed at the Naval Research Laboratory (NRL) on the Gamble II generator under Defense Nuclear Agency (DNA) auspices, to the higher power and longer pulse length of the PITHON generator at Physics International Co. (PI). A collaborative effort between NRL and PI was carried out with DNA support under contract DNA 001-79-C-0023 at PI and contract DNA Subtask TAQAXLA014 at NRL. The DNA contract officers were J. Z. Farber and R. L. Gullickson.

Experimental measurements on the PITHON generator were carried out in two 4-week sessions during Aug.-Sept. 1979 and April-May 1980. A total of 46 shots were fired in the first session and 41 shots in the second session. Analysis of the data accumulated from these shots has continued up to the present time.

The extensive set up of diagnostics on the experiment and the detailed data analysis has involved the support of the following personnel. Lead technician H. J. Kishi at PI designed and directed hardware construction and assembled the diode hardware on each shot in the first pulsing session. During the second session T. Robinson of NRL was responsible for the diode assembly. B. Hartneck of PI supported operation of the laser holographic system. The transfer of data to NRL and the development of software routines for data analysis was carried out by D. Bacon and D. Hinshelwood of NRL. Finally, the support and encouragement of PI management including A. J. Toepfer, S. Putnum and K. Childers in carrying out this collaborative effort is gratefully acknowledged.

PRODUCTION OF INTENSE LIGHT ION BEAMS
FROM A SUPERPOWER GENERATOR

I. INTRODUCTION

Recent technological advances in the production and focusing of intense pulsed light ion beams (hydrogen, deuterium, and carbon) have raised the attainable intensities from levels of 1 A/cm^2 into the MA/cm^2 regime.[1-3] The present achievements of high-power ion beams and the potential for continued advancements in this field make them prime candidates as drivers for inertial confinement fusion (ICF). Requirements of an ICF system that are met by an ion beam driver[4-6] include: (1) ions can be produced at high efficiency in extraction geometries appropriate to ICF ignition,[7-9] and (2) beam power density delivered on target can be significantly larger than the source density through velocity bunching of the ions during transport,[10] by geometrical shaping of the ion source,[8] or by externally magnetically focusing the extracted ion beam.[7] A specific advantage of an ion beam driver for ICF is that the ion energy deposition profile in the target is more favorable than those of either laser photons or relativistic electrons[11].

A variety of diode configurations to produce light ion beams for ICF have been discussed in the literature.[1] In this paper, experimental investigations into the production and ballistic focusing of proton and deuteron beams from one such diode are presented. The pinch-reflex diode,[8] developed by the Naval Research Laboratory (NRL) on the Gamble II accelerator, was matched to the PITHON generator[12] at Physics International Company. In addition to diode physics studies, the coupling between a biconic magnetically insulated vacuum transmission line and a small pinch-reflex diode at high stress (E > 2 x 10^6 V/cm) has been investigated.

The early motivation for this work stemmed from computational modeling of the pinch-reflex diode toward ICF applications. The PITHON generator parameters may satisfy requirements for a single module in a multi-ion-beam target irradiation concept based on beam bunching during transport in Z-pinches[13] and multi-beam overlap on target. Two experimental sessions were performed with this generator: The first studied the scaling of diode performance and ballistic focusing at higher powers and longer pulselengths than previously available;[2] the second studied the detailed shape evolution of the electrode plasma surfaces--information essential for design of a diode to produce a high quality focused ion beam.[14]

In this paper we present the results of these studies. The generator and diode are discussed in Sec. II. The beam diagnostics employed to evaluate ion species, current density profile and history, time-integrated beam geometry, and anode plasma surface evolution are described in Sec. III. The principal results of the two experimental sessions are presented and discussed in Sec. IV. Conclusions of this work are presented in Sec. V.

II. EXPERIMENTAL APPARATUS

A. Accelerator

The PITHON accelerator, shown schematically in Fig. 1, is a water dielectric multi-stage coaxial transmission line driven by a 40-stage, 1.5-MJ, oil-insulated, twin Marx generator. The 2.3 Ω intermediate storage capacitor is charged to a voltage above the open circuit Marx potential (through ringup), then discharged via a single-site, self-breaking water switch into a 1.3-Ω pulse forming line (PFL). Multi-site water output switches provide a low-inductance energy transfer from the PFL to a tapered 1.0 Ω first transformer in a pulse of about half the PFL voltage and twice the duration.

A common problem in pulsed power accelerators is a low-voltage, long-duration "prepulse" loading the diode prior to the main high voltage pulse. This phenomenon is due to capacitive coupling between sequential inner conductor stages of the accelerator and can often lead to diode shorting and nonreproducibility. This coupling is reduced in PITHON by a low permittivity epoxy "prepulse slab" between the first and second transformers (see Fig. 1). For a shot yielding a 2-MV output pulse, this technique reduces the prepulse level at the vacuum interface from over 300 kV to below 10 kV thus allowing the use of a wide variety of field-emission-diode loads.

Multi-site, gas-insulated switches connecting the transformers through the prepulse slab close on the leading edge of the high voltage pulse. There are two interchangeable second transformers which connect this slab to the water-vacuum interface with characteristic impedances of 0.75 and 1.0 Ω. Both interfaces allow penetration of a "transit time isolator" cable shield through the water from the high-voltage vacuum cathode to the grounded outer shell. Through this isolator the ion-beam diagnostic signals, floating at the 2- to 2.5-MV cathode potential, can be extracted with less than 50-mV noise.
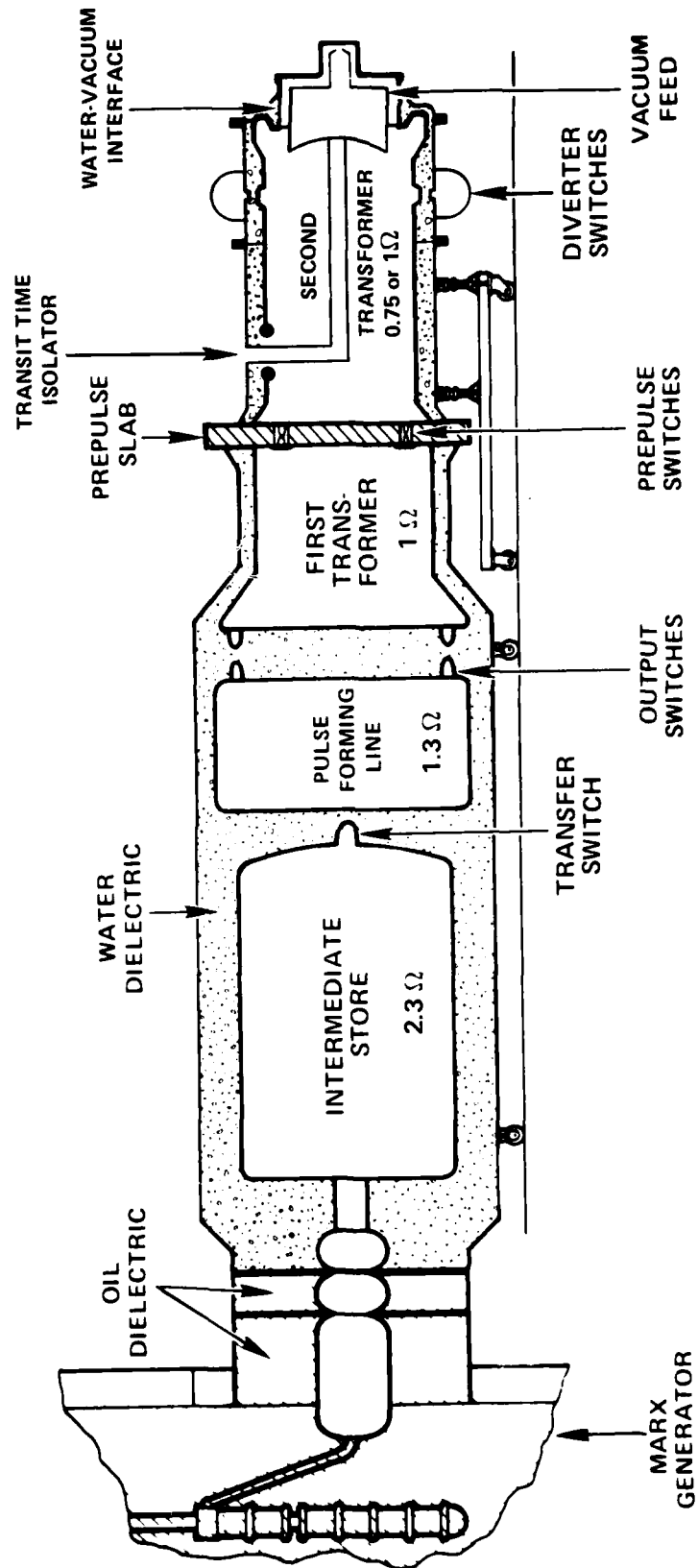
Fig. 1 — Schematic of the PITHON waterline

The vacuum feed connecting the second transformer to the diode is shown in Fig. 2. The shaded area is the water-dielectric transmission line, which carries the electromagnetic wave. The line bends radially inward and flares to reduce the electric field stress on a graded axially-stacked epoxy interface separating water from vacuum. Interface voltage and current diagnostics (V_T and I_T) are located at the flare in several azimuthal locations. On the vacuum side of this interface, the energy pulse is carried by an electromagnetic wave and by electrons. The total current can be measured on the anode and is monitored at the vacuum interface (I_0) and at the diode (I_D). The total inductance between these monitors is about 30 nH. A dielectric surface flashover switch interrupts the cathode side of the feed to further reduce the prepulse on the diode to about 5 kV.

B. Diode Structures

Two independent cathode and anode configurations were tested in these experiments. The diode structures used in the first run are shown in Fig. 3. Following the vacuum feed from the flashover switch toward the axis, a sudden transition is made from a radial biconic to a coaxial feed. The center conductor is the cathode shank, a 0.6-cm-thick wall stainless-steel cylinder. The outer coax anode shell is aluminum and can be adjusted for concentricity and axial spacing. This coax section terminates in the pinch-reflex diode: a thin hollow cathode tip opposite a grounded planar or spherical anode.

A planar pinch-reflex diode is shown in Fig. 3a. The anode assembly is a disk of 0.012-cm-thick polyethylene (CH_2) held 5 mm from a carbon backing plate by an outer insulating annulus and a central carbon button. When this foil flashes early in the electrical pulse, an anode plasma spreads across the foil and expands into the anode-cathode gap. Ions are accelerated toward the cathode from the low-density front of this moving plasma and are deflected radially inward by their self-magnetic field toward a time-varying collection of foci. The ion beam current (I_{ion}) is measured by a Rogowski coil sheltered behind the cathode tip. The ions entering the cathode pass through a 1.8-μm-thick polycarbonate (Kimfol*) foil pressure window and propagate current- and charge-neutralized in a 1-Torr-nitrogen drift chamber.

*available from Kimberly Clark Corp., Lee, MA, 01238
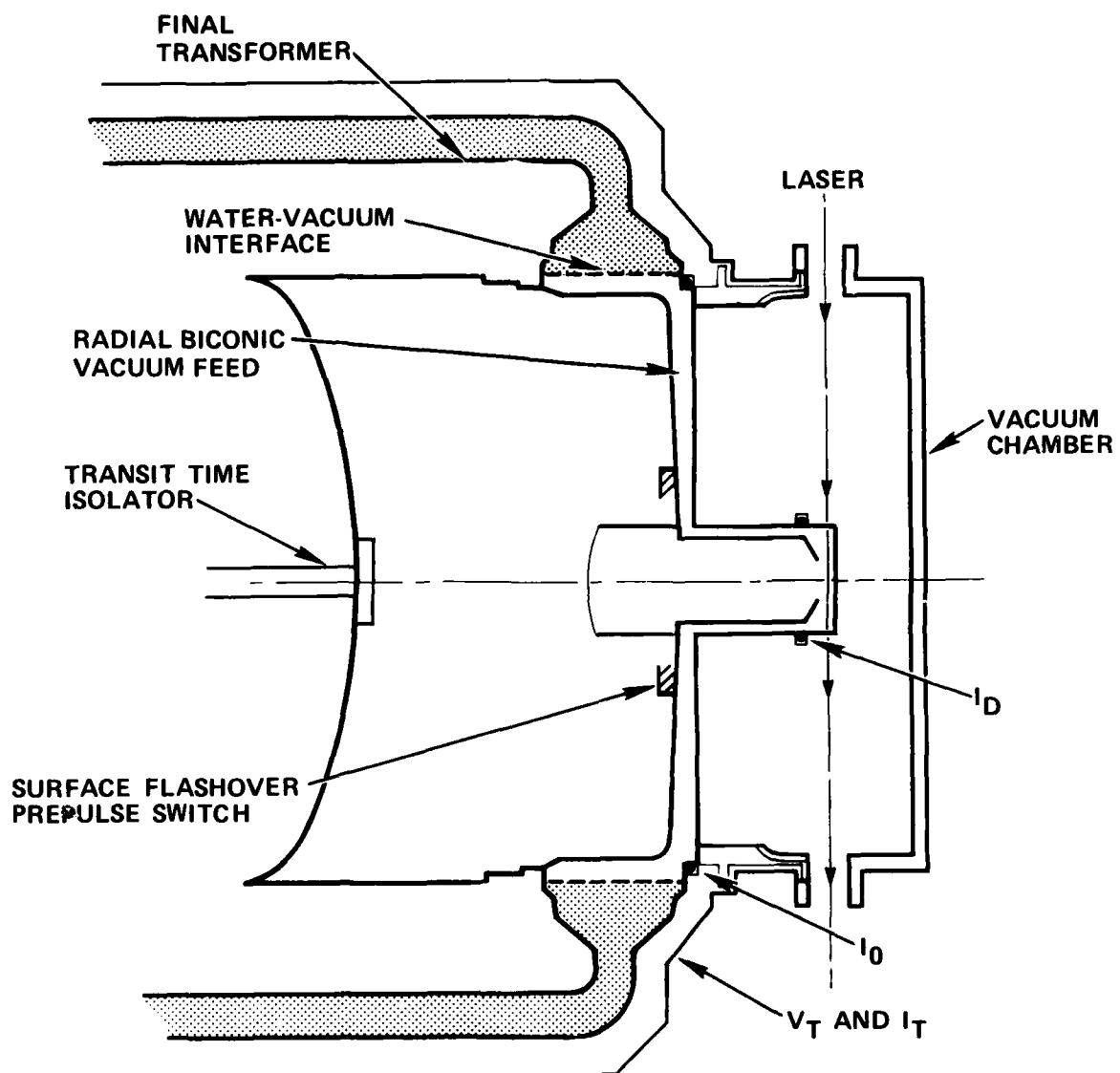
4

FINAL TRANSFORMER

LASER

WATER-VACUUM INTERFACE

RADIAL BICONIC VACUUM FEED

VACUUM CHAMBER

TRANSIT TIME ISOLATOR

I_D

SURFACE FLASHOVER PREPULSE SWITCH

I_0

V_T AND I_T

Fig. 2 — Schematic of the vacuum feed interface on PITHON

(a)

DIELECTRIC FLASHOVER SWITCH

BICONIC VACUUM FEED

I_D

6.4 mm 6061 Al WITNESS PLATE

CATHODE TIP

CARBON ANODE BACKING PLATE

PLASTIC ANODE FOIL

KIMFOL PRESSURE WINDOW

1 torr N_2 GAS-FILLED DRIFT REGION

GAS BAG

I_{ION}

(b)

I_D

SPHERICAL ANODE BACKING PLATE

I_{NET}

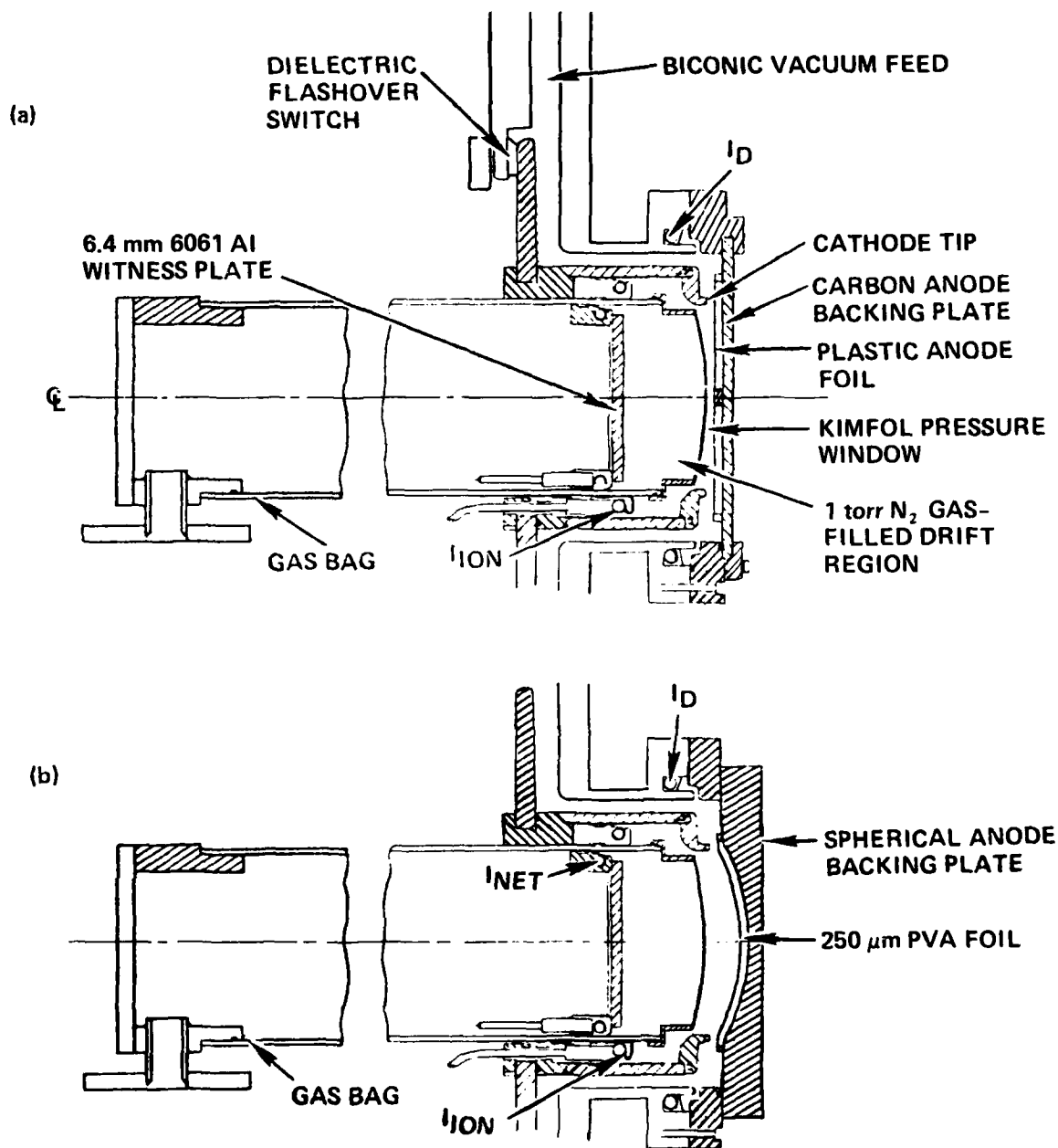250 μm PVA FOIL

GAS BAG

I_{ION}

Fig. 3 — Pinch-reflex diode assemblies for the first experimental session in (a) planar geometry and (b) focusing geometry

The focusing configuration of the pinch-reflex diode in the first experimental session is shown in Fig. 3b. Anode foils of 0.025-cm-thick polyvinyl-acetate (PVA), deformed into a spherical section with a 12.7-cm radius-of-curvature, were mounted onto similarly machined carbon backing plates to maintain a 5-mm foil-plate separation (see Fig. 3b). An extended tip cathode was used to define the 100-cm^2 diode area for pinch-reflex electron operation with a 3- to 4-mm anode-cathode gap. The initial ion velocity is directed toward a geometric focus located substantially inside the planar-diode focal length. The intent of this design is to create a high-current-density ion-beam focus which is less sensitive to self-deflection variations during the pulse[14] and from shot to shot.

The diode structures used in the second session were somewhat different from those shown in Fig. 3 and are displayed in Fig. 4. The coax gap was increased to form a higher inductance but constant characteristic impedance 5-Ω transition from the biconic into the coaxial feed. This design represents an attempt to improve the vacuum power flow into the diode structure. The thick stainless-steel cathode shank was severely distorted after a few PITHON shots in the first run and has been replaced with disposable spun aluminum cylinders in this design. By sealing the inner cathode volume with Kimfol glued to the tip of the ion Rogowski assembly, the inside of the cathode is pressurized to 1-Torr nitrogen while the surrounding volume is at ambient 10^{-5} Torr pressure. Variation of cathode radius was engineered by spinning a smooth taper on the cathode tip. Figure 4a shows a 100-cm^2 cathode bore, while Fig. 4b shows a smaller 30-cm^2 area diode.

The coax length was extended to allow access for direct viewing across the diode gap with a ruby laser holographic system. Planar diodes were used and disposable anode backing plates were fabricated of spun aluminum in which an array of viewing slots were machined. The slots were made as symmetric as possible consistent with direct viewing to avoid return current asymmetries. Finally, a 7.6-cm-diam central carbon insert was pressed into the backing plate to minimize bremsstrahlung and to reduce aluminum buildup on the reusable diode hardware.
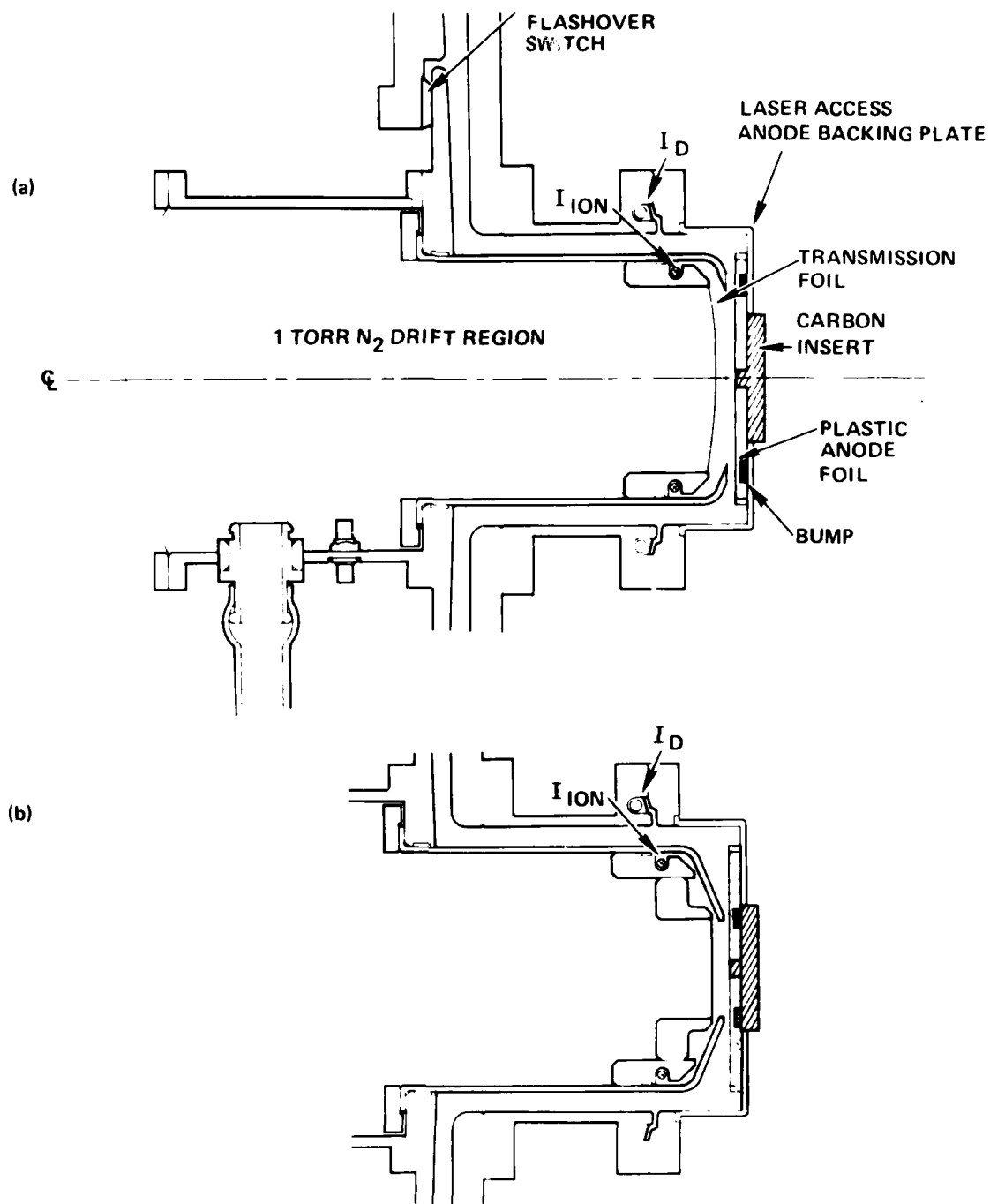
Fig. 4 — Pinch-reflex diode assemblies for the second experimental session for (a) a 100-cm^2 area diode and for (b) a 30-cm^2 area diode

8

III. DIAGNOSTICS

In this section the generator, beam, and plasma diagnostics will be described and data reduction procedures will be discussed. These include: generator voltage and current detectors distributed in the vacuum feed; bremsstrahlung diagnostics for the electron-beam pinch history and time-integrated x-ray profile; a Rogowski coil to measure the ion-beam current; a "shadow box" diagnostic for spatial-profiling of the ion beam; nuclear-reaction diagnostics for ion-beam duration and fluence; and interferometric laser holography for evolution of the anode and cathode plasmas.

A. Electrical Measurements

The accelerator diagnostics for voltage and various currents are shown in Fig. 2. The injected voltage is measured by balanced capacitive dividers (V_T) at several azimuthal locations in the water, displayed separately to evaluate wave symmetry, and averaged to calculate impedance, power and energy. The injected current is monitored both in the water adjacent to the voltage probes (I_T) and in the vacuum (I_0) at the entrance to the radial biconic transmission line with dB/dt and segmented Rogowski probes, respectively. The difference between these measurements affords insight into water or vacuum arcs in the interface and transition regions. The total diode current (I_D) is measured with a self-integrating Rogowski coil[15] as is the ion current (see Figs. 3 and 4). These current monitors have risetimes of less than 5 ns and integration times greater than 3.4 µs . Several designs are employed to shield the epoxy encapsulated coils from particle bombardment and UV irradiation while minimizing the monitor inductance. On most shots, valid ion current measurements are obtained from power onset to peak. All current monitors are bench tested and cross-calibrated in short circuit shots. The data are monitored through a 200-MHz bandwidth 7912R transient digitizer system controlled by a PDP 11/40 computer and are reduced numerically.

B. X Rays

The ion power and energy on each shot are qualitatively correlated with the yield of bremsstrahlung radiation and the symmetry and size of the electron pinch as evidenced by its x-ray image. Because the bremsstrahlung yield scales with diode potential, a large x-ray signal with a large FWHM (40-60 ns) indicates a high-voltage, long-impedance-lifetime shot.

9

The time-resolved x-ray output from the electron pinch is monitored with an optical photodiode (PDX) coupled to a plastic scintillator. The unit is rigidly mounted outside the vacuum chamber at 180^0 to the diode axis. Similarly mounted is an x-ray pinhole camera to record hard photons (E > 30 keV) from the diode region through a 0.05-cm-diam 20^0 tapered pinhole. This camera images the diode onto a stack of Kodak No-Screen, XR5, and Polaroid Type 52 films coupled to a variety of intensifier screens. This wide range of film sensitivities to x rays affords good contrast over the variation of bremsstrahlung intensity across the diode image. Lithium fluoride thermoluminescent detector (TLD) capsules monitor the time-integrated bremsstrahlung dose at the photodiode from the entire anode. Serious current losses in the vacuum feed were correlated with the photographic, TLD, and PDX data as well as with visual damage following a shot.

C. Ion Imaging

The location of the ion-beam focus was determined by using ballistic reconstruction of ion trajectories from the edges of ion-induced melt damage patterns recorded on the rear witness plate of a shadowbox[2] (see Fig. 5). The interpretation of this data is based on several key assumptions. These are: the ions are accelerated from a planar anode plasma with initial velocity vectors parallel to the axis; as they cross the anode-cathode gap each ion is magnetically deflected by the field of a calculated ion-current-density profile.[16] Upon crossing the cathode foil and entering the 1-Torr-nitrogen drift chamber, the ions are assumed to be charge and current neutralized and hence execute straight-line orbits through a focal region and expand into the shadowbox. The current neutrality premise has been verified by measurements of the net-current fraction in the gas (I_{net}/I_{ion}) of less than 2% on both Gamble II (Ref. 2) and PITHON. The damage patterns on the witness plate of the shadowbox are projections of the ion beam through the front apertures (see Fig. 5). The patterns, which are time-integrated records, often form teardrop or oval shapes. The radial variation is attributed to the change in focal length during the pulse due to time-varying diode fields. The azimuthal width of the damage is due to the divergence of the ion beam from the anode plasma, asymmetries in the source, and scattering through the transmission foil. The computer reconstruction, shown in Fig. 5, traces the recorded damage areas back through the front-plate apertures, through the focus, and onto the anode
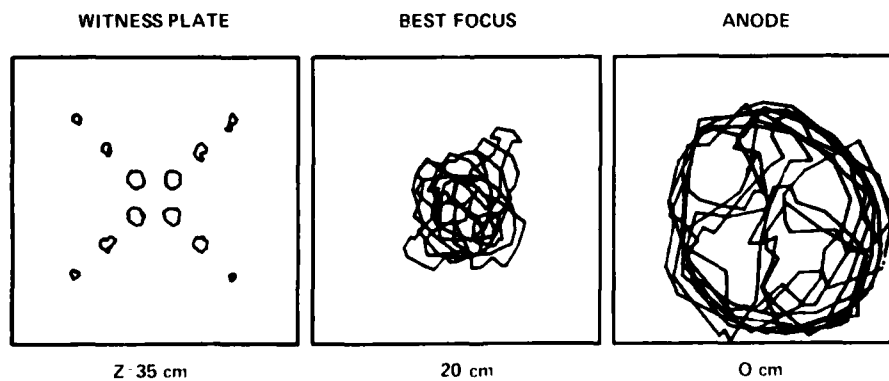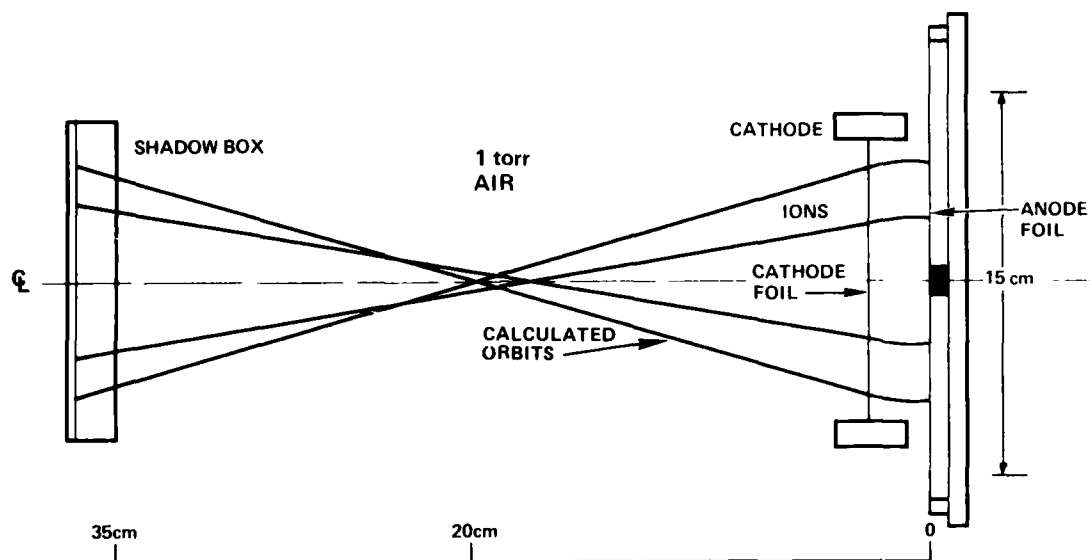
Fig. 5 — Shadowbox geometry and reconstruction of ion-beam
trajectories for planar-diode Shot 1676

surface. The large damage patterns at the smallest radii on the witness plate are due to the time-varying focal spot moving through the shadowbox location and are not useful in planar geometry reconstructions.

D. Nuclear Diagnostics

The intensity and duration of proton or deuteron currents were also monitored by nuclear-reaction techniques. For proton beams, a prompt γ-ray diagnostic[17] was employed utilizing the $^{19}F(p,\alpha\gamma)^{16}O$ reaction. Teflon (CF_2) targets were placed in the ion-beam path, and 6-MeV prompt γ rays were measured with a fast scintillator (NE-111) and photomultiplier (XP-2020) detector housed in a 3.2-cm-thick lead enclosure located 4 m from the ion diode at 95° to the diode axis behind a one meter-thick concrete shielding wall. This wall differentially shields the diode bremsstrahlung and improves the γ-ray-to-bremsstrahlung ratio. Measured and calculated signals for this detector on a shot with a CH_2 anode and Teflon target are compared in Fig. 6. This detector could not be calibrated absolutely as the attenuation of the prompt-γ signal by the concrete shielding wall is difficult to estimate.

The total yield of deuteron beams was determined by measuring neutrons from the $D(d,n)^3He$ and $^{12}C(d,n)^{13}N$ reactions. Deuteron beams, produced by using CD_2 coated PVA foil anodes, were directed onto thick CD_2 targets to produce these reactions. Because the ion beam was directed into the generator in these experiments, neutron measurements were confined to recoil angles greater than 90°. Total neutron yields were measured with two rhodium activation detectors[18] located 17 m from the diode at 175° to the diode axis. These detectors viewed the diode through a 30-cm-diam hole in a concrete shielding wall located 8.3 m from the diode. This geometry minimized the number of room-scattered neutrons which reached the detectors and allowed the intensity of the direct collimated neutron beam to be scaled inversely with the square of the source-to-detector distance, even at 17 m. These rhodium activation detectors were calibrated with a ^{252}Cf neutron source as described in Ref. 18. Deuteron intensities were inferred from measured neutron intensities by using $D(d,n)^3He$ and $^{12}C(d,n)^{13}N$ reaction yields. Thick-target yields for these reactions were calculated from measured cross sections[19,20] and published stopping powers[21] and are presented in Fig. 7. Above 1 MeV, the $^{12}C(d,n)^{13}N$ reaction contributes significantly to the neutron yield.
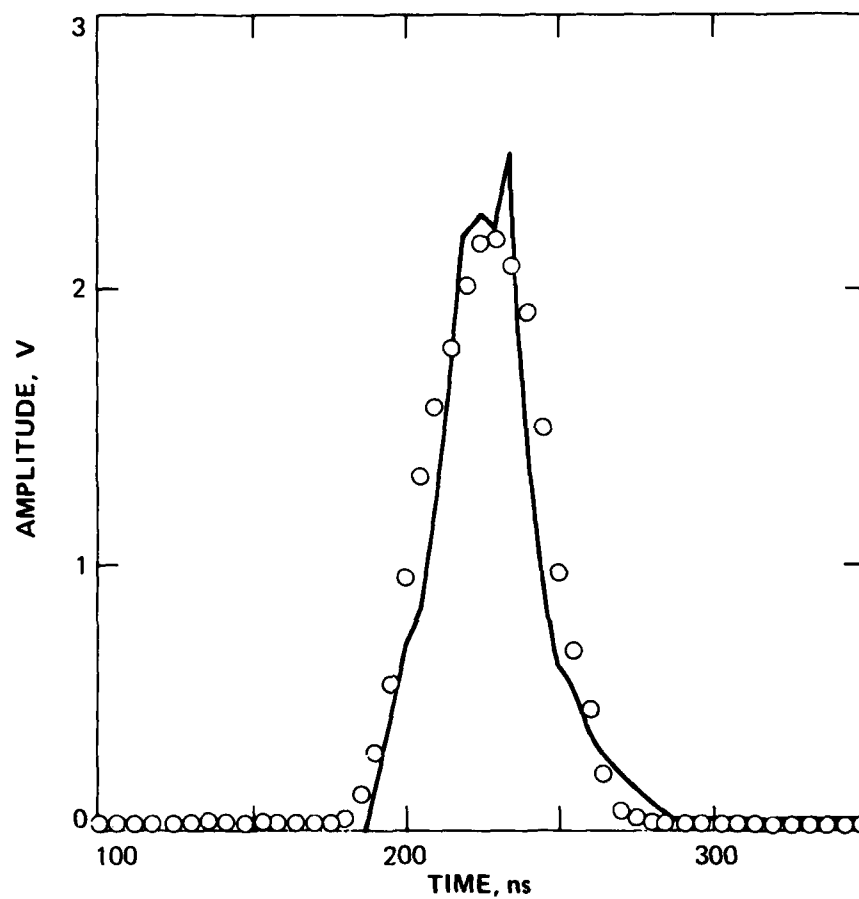
Fig. 6 — Prompt-γ signals measured on Shot 1665 (solid line) and calculated (open circles) for protons on a thick CF_2 target. The calculated trace has been normalized in amplitude to the measured signal. Good agreement in pulse width and shape is shown.
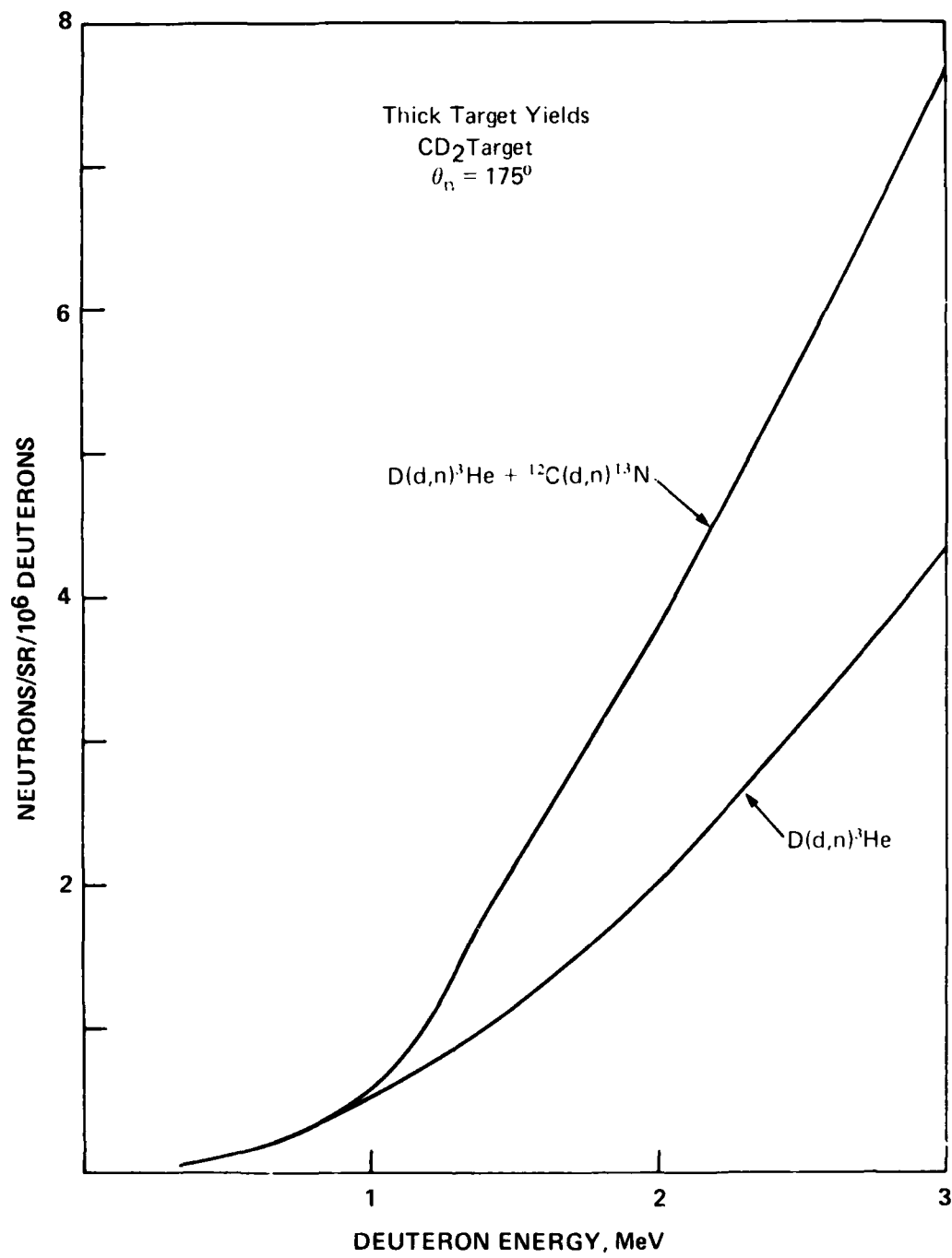
13

Fig. 7 — Thick-target yields for the $D(d,n)^3He$ and $^{12}C(d,n)^{13}N$ reactions at 175°

14

The neutron time-of-flight (TOF) technique was used with the $D(d,n)^3He$ reaction to determine neutron energies and to monitor the duration of the deuteron beam. Neutron energies were determined with a TOF detector located 16.8 m from the diode in the same geometry as the rhodium activation detectors. This detector consisted of a fast scintillator (NE-111) quenched with 5% piperidine[22] and photomultiplier (XP-2020) mounted within a 7.6-cm-thick lead shield. To operate this detector in the linear range, the light incident on the photomultiplier was attenuated with an ND-1 filter. The time history of the deuteron beam was determined using a TOF detector with a relatively short flight path as described in Ref. 23. For this purpose, a detector was located 3.2 m from the diode at 160° to the diode axis. This detector consisted of a similar fast quenched scintillator (NE-111), an ND-2 filter, and a photomultiplier (XP-2020) mounted within a 10-cm-thick lead shield. Typical traces from these two TOF detectors are shown in Fig. 8 along with calculated neutron pulse shapes for these detector locations. For the detector at 16.8 m, the time interval from the peak of the bremsstrahlung to the peak of the neutron signal was used to determine the neutron energy. An energy of 1.9 ± 0.2 MeV, consistent with the diode voltage, was determined from this trace after correcting for the x-ray flight time. For the detector at 3.2 m, the duration of the neutron signal gives a measure of the duration of the deuteron beam. The width (FWHM) of this neutron pulse is 60 ns, which compares favorably with the duration of the ion pulse based on the measured diode voltage and ion-current traces for this shot.

E. Interferometric Holography

The final diagnostic to be described is the interferometric holography system[24] used to monitor the anode and cathode plasma motions in the interelectrode gap. The system configuration is schematically illustrated in Fig. 9. The system employs a 6-ns ruby laser pulse, which is split into four beams. These are delayed by path length into 10-ns increments to form a train of four laser pulses over a 30-ns interval. Each of these four beams is split into a scene and reference beam. Each scene beam passes through the pinch-reflex diode and then through lenses and mirrors to form a real image of the diode on a glass holographic film plate. The reference beams are directed to the film without passing through the diode, overlapping their respective scene beams to produce an array of four holograms on the film plane. Two such sets
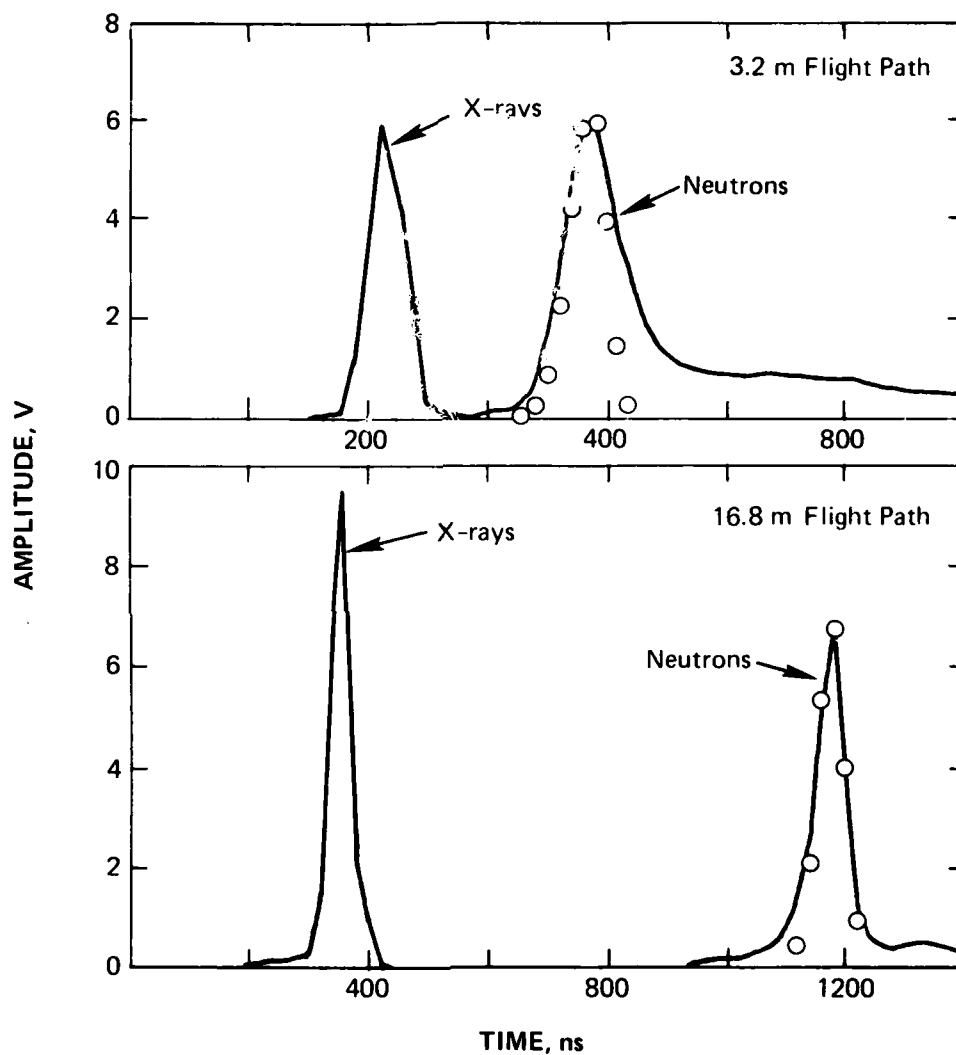
15

Fig. 8 — Neutron TOF traces for Shot 1692. Calculated neutron pulse shapes at 3.2 m and 16.8 m are plotted as open circles. The calculations are normalized in amplitude to the measured neutron responses.
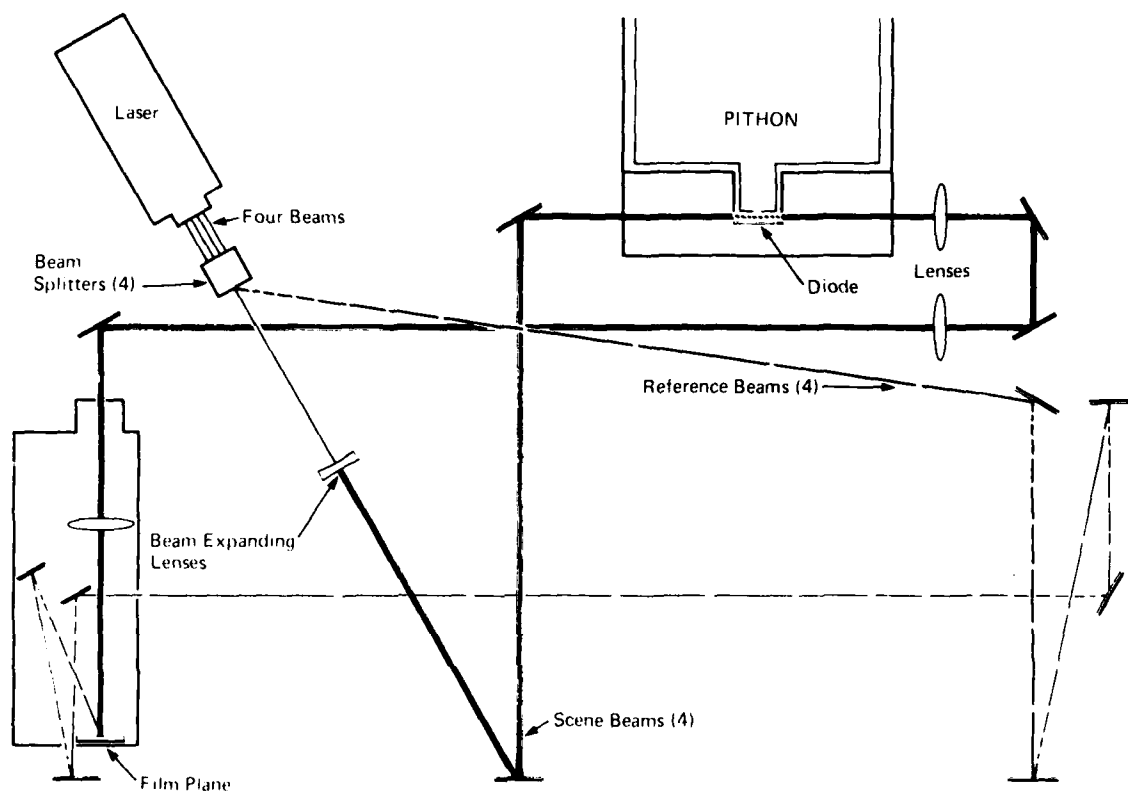
16

Fig. 9 — Ion-diode laser interferometric holography system

of holograms are superposed: one made before the shot and the other during the shot. The two sets of interference patterns overlap to form four Moire patterns. The differences between a superposed pair of holograms are due to optical-path-length variations in the scene beam where it passes through the diode plasma.

By shining light through a developed interferometric hologram, both an image of the diode and series of fringes can be seen. As an aid to data interpretation, a uniformly changing optical-path-length difference between the two hologram sets is introduced by slightly tilting one of the mirrors in the system after the first set is exposed. This produces a reference array of uniformly spaced straight fringes on the image where no plasma is present. Additional changes in the optical path length caused by plasma result in bending of the fringes: the bending of a fringe over the distance of one reference fringe spacing corresponds to an additional wave length of path difference due to the plasma. The corresponding plasma density can be estimated by the relation:

$$n_e \, \Delta X = 3.2 \times 10^{17}/cm^2/\text{fringe shift}$$

where ΔX is the total path length through a uniform plasma of density n_e. The largest plasma line density measurable by this technique is that for which the index of refraction equals zero (i.e. $2.3 \times 10^{21}/cm^2$). The maximum density observable in this experiment is estimated to be between 10^{19} and 10^{20} due to ray-tracing effects: large-angle refraction of the laser beam by higher-density plasmas reduces the light intensity entering the optical system and the exposure level on the film.

Unfolding the detailed radial-density profile is not possible with this technique. Figure 10a shows the diode area with the laser-viewing slots machined out of the anode: the shaded area is the laser-beam cross section, and the clear holes are the observable diode regions. It is important to note that the view through a hole pair is a chord across a disk system which may not be axially symmetric: a thin plasma ripple in an orientation other than the laser axis will appear to be a large-area plasma motion. Further, anode plasma which crosses the visual anode-cathode gap inside the cathode inner radius does not necessarily contact the cathode plasma lifting off the hollow

18

(a)

(b)
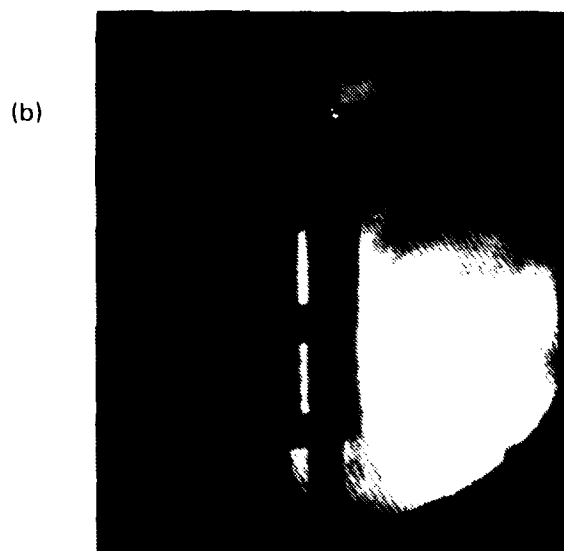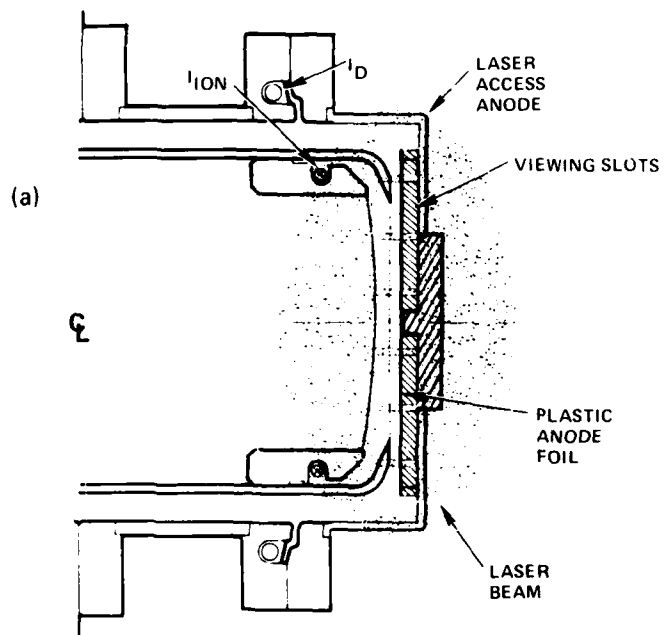
LASER PHOTO

Fig. 10 — (a) Ion-diode laser diagnostic detail, and
(b) reconstructed holographic interferogram

emission ring. Despite these limitations, the system presents new information about the plasma surface evolution which is important for the design of high-focus-quality diodes.[25]

IV. EXPERIMENTAL RESULTS

A variety of experimental goals were addressed in the two pulsing sessions. The first session extended scaling of the pinch-reflex ion diode to the higher power and longer pulselength of the PITHON generator. Both planar and spherical anode foils were tested. The second session utilized modified accelerator impedance and vacuum feed hardware. Emphasis was placed on determining the electrode plasma evolution in the diode, the scaling of diode parameters with cathode radius, and the consequences of diode modifications.

A. Planar Diode Experiments

The important scaling parameters studied in these experiments were the ion efficiency, the ion turn-on time, and the diode-impedance lifetime. The PITHON generator was chosen for these scaling studies for its similarity to Gamble II in minimal prepulse, similar impedance (1.0 versus 1.5 Ω) and voltage risetime, yet larger peak voltage and pulsewidth. These similarities suggested the physics of the pinch-reflex diode would be the same and detailed comparisons could be made between equivalent power PITHON and Gamble II shots. These comparisons, performed during the first session, confirmed the baseline similarity between the accelerators. The scaling variables are then the 70% larger and 30% longer FWHM power pulses available on PITHON. Theoretical calculations[8] based on the generator open-circuit-voltage waveforms predicted a doubling of the Gamble II ion currents to about 1.0 MA of protons from a pinch-reflex diode on PITHON.

A typical waveform data set from the first experimental session (Shot 1662) is shown in Fig. 11. The injected voltage and current measured at the water-vacuum interface (see Fig. 2) have 2.1-MV (V_T) and 2.0-MA (I_0) peak values at a mean impedance of 1.2 Ω. These signals indicate a 4-TW power pulse of 88-ns FWHM containing 340 kJ is injected into the vacuum feed structure. The voltage impressed on the diode (V_D) is less than the injected voltage by the L(dI/dt) inductive drop due to the wave passing through the
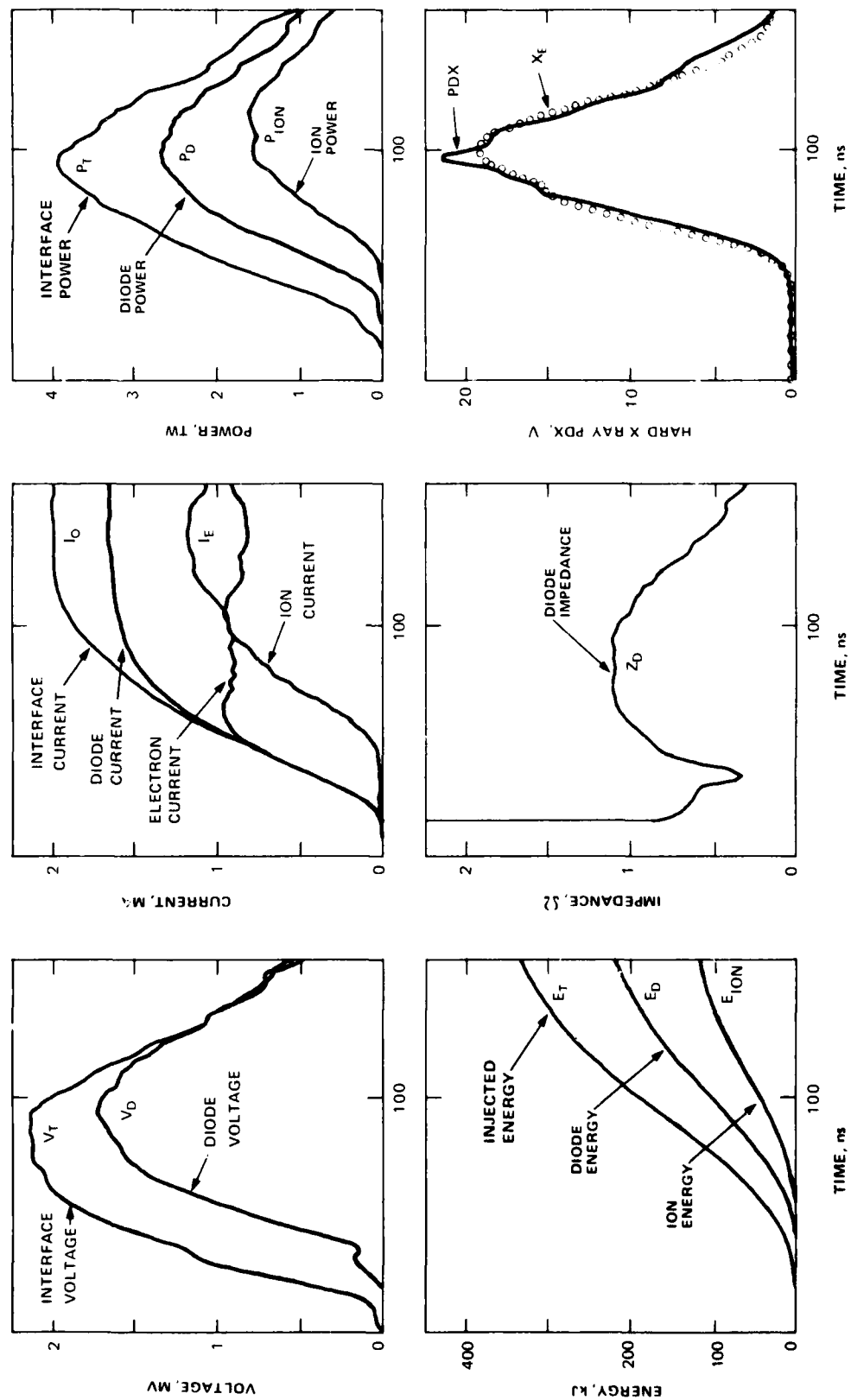
20

Fig. 11 — Measured waveforms for Shot 1662 at 4 TW

vacuum feed. The effective inductance is determined to be 30 nH by defining the potential across a shorted diode to be zero. There is a current loss in the vacuum feed shown by the difference between the interface (I_0) and diode (I_D) current waveforms. The total electron current in the system (I_E) is defined as the difference between the interface (I_0) and ion (I_{ion}) currents. Despite the losses in the vacuum feed, 2.7 TW and 230 kJ were coupled into the diode on this shot. The ion-beam current entering the 100-cm^2 cathode bore (0.9 MA at 1.7 MV) begins 22 to 26 ns after the diode current, a delay characteristic in all these experiments. The resulting peak ion power and energy are 1.6 TW and 125 kJ respectively. These data correspond to an average source current density of 12 kA/cm^2, which is in agreement with numerical predictions.

The diode-impedance lifetime is an important consideration in scaling the ion diode toward an eventual ICF application. The velocity bunching desired for power multiplication requires carefully programmed voltage and impedance histories. The diode impedance shown in Fig. 11 reaches a plateau near 1.1 Ω for 40 ns then slowly falls until the end of the applied pulse. Accurate impedance control was provided by anode-cathode gap adjustment, with shot-to-shot variations of 0.2 Ω obtained throughout the experimental sessions.

The ion Rogowski coil located inside the cathode provided timing of the formation of an anode plasma on the cathode side of the anode foil. Frequently a low-level signal is seen starting with the diode current (see Fig. 12), due perhaps to a small anode-foil hot spot or to electrons emitted from the ion Rogowski holder and transmission foil. Several explanations for the 22 to 26-ns delay for ion turn-on are possible. One conjecture, based on pinched-electron-beam-diode physics[26] is that before the anode foil flashes, forming a plasma and bringing the floating dielectric foil to ground potential, the electron beam passes through the anode foil and pinches on the backing plate. Previous pinched-electron-beam experiments[27] on PITHON have measured pinch areal velocities of 5 cm^2/ns, or a value of 20 ns for the present 100-cm^2 experiments, which is consistent with the measured delay. The resulting high field stress on the foil adjacent to the central button could then cause surface flashover. If this mechanism is responsible for anode-plasma formation, the small-area (30 cm^2) diodes tested should exhibit a much smaller delay in ion turn-on time of roughly 8 ns. These results, presented
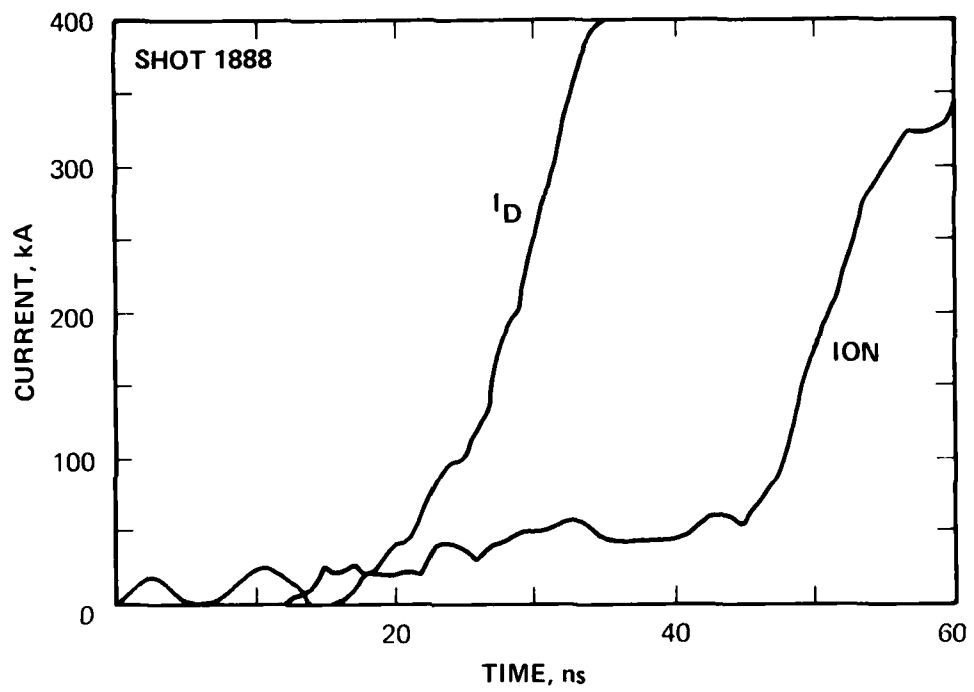
Fig. 12 — Early-time behavior of the diode- and ion-current traces

later, show no discernible change in the delay of ion turn-on. An alternative explanation for the ion delay is that it represents the inherent delay of surface flashover.[28] For these large and small area diodes, the difference in delay would be ± 5 ns which is within the shot-to-shot variation.

The radiation diagnostics provide corroboration of the relative timing and waveshape of the diode voltage, injected current, and ion current. The x-ray photodiode signal (PDX) for Shot 1662 is shown in Fig. 11 and compared with a calculated waveform (X_E). The theoretical scaling[29] for x-ray production from electron beams is given by $X_E = I_E(V_D)^{2.8}$, which is a sensitive measure of voltage waveshape. The calculated waveform was normalized in magnitude and shifted in time for the comparison, and the shapes of the two signals agree reasonably well. This agreement provides an independent check on how well the measured voltage and electron current pulse shapes represent the actual wave shapes at the diode. Similarly, the agreement between the measured and calculated prompt-γ nuclear radiation signals[17], shown in Fig. 6, indicates that the diode voltage and ion current pulse shapes are correctly timed and are of reasonable proportion.

The ratio of the ion current to the diode current provides a direct measure of the pinch-reflex-diode efficiency for ion production. At maximum power the efficiency on Shot 1662 is 60% for an ion current of 900 kA. Bremsstrahlung measurements, as described in the next paragraph, indicate that the electron beam formed a well-centered pinch with good coupling of the injected energy to the diode on this shot.

Bremsstrahlung diagnostics were used to study the symmetry of power flow and current loss in the vacuum feed and diode regions. Measurements for two different classes of shots are compared in Fig. 13. A well-centered pinch with bremsstrahlung from only the central 2 cm of the 12-cm-diam anode is observed in the x-ray pinhole photograph in Fig. 13a. For this shot, the x-ray photodiode signal (PDX) is substantial for the entire diode pulse duration, and the energy at the vacuum interface (E_T) shows good coupling of the injected power to the diode. A second class of shots is shown in Fig. 13b where the power flow is asymmetric and the electron pinch is not well centered. The x-ray pinhole image shows flutes extending onto the aluminum backing plate, and bremsstrahlung from the coax feed at 9-cm radius is seen. Intense bremsstrahlung emission from aluminum and stainless steel, relative to
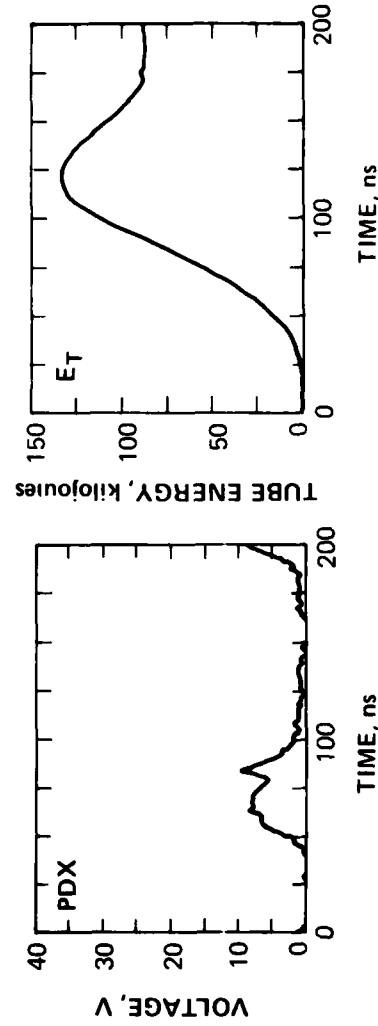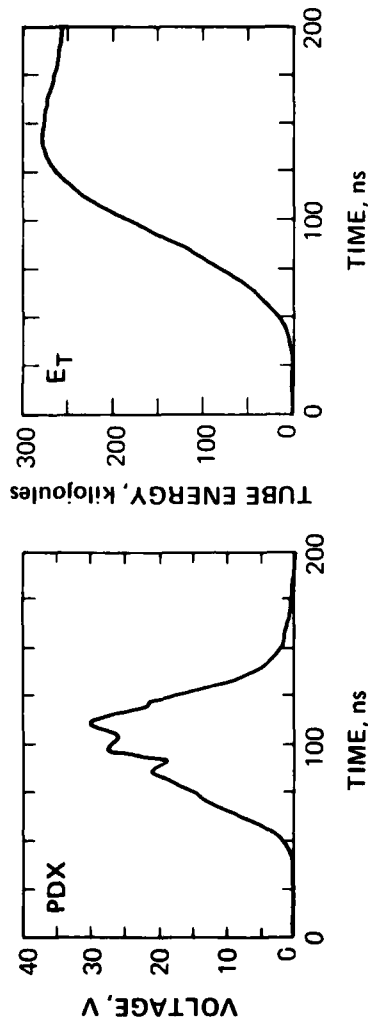
Fig. 13 — Comparison of x-ray pinhole images, x-ray photodiode traces and total energy at the vacuum interface for shots with (a) a good quality pinch and (b) a poor pinch

carbon, allows electron losses in the vacuum feed at low current density to have intensities comparable to the intense central pinch on carbon. On this shot the PDX trace is smaller in amplitude and narrower in pulsewidth, indicating a reduction in diode voltage. Also, a significant fraction of the injected energy is reflected off the load. Visual damage to the feed hardware was consistent with the origins of x rays indicated in Fig. 13 on these two shots.

The shadowbox diagnostic was used to determine the time-averaged location and size of the focus as indicated previously in Fig. 5. A model developed to predict the best focus location[14] yielded a minimum spot size at about 18 cm from the anode foil for the voltage and current values of a typical 3-TW shot. The ballistic reconstruction shown in Fig. 5 gives a best focus at 20 cm, in good agreement with this prediction. Witness plate targets of 6.4-mm-thick aluminum (6061-T6) placed at this location showed centered front surface damage and backspalls about 1 cm in diameter (see Fig. 14).

B. Focusing Diode Experiments

Experiments investigating geometric focusing of high power ion beams from a pinch-reflex ion diode, which were first performed at NRL on Gamble II (Ref. 8), were extended to higher power in the present experiments on PITHON. It is important to note that the voltage, current, and impedance characteristics of the focusing diodes are essentially the same as those of the planar diodes. The ions are magnetically deflected in passage across the anode-cathode gap, then drift ballistically in the 1-Torr gas to an actual focus at about 9 cm from the anode foil, inside the geometric focus located at 12.7 cm. This magnetic bending is demonstrated by shadowbox reconstructions shown in Fig. 15. The damage patterns extrapolate back through the focus to cover the entire anode plane. The focal spot is seen to be within a 3-cm-diam circle, corresponding to an areal beam reduction from the anode source of 14. A preliminary estimate of the focused current density can be made by assuming the entire measured ion current is uniformly distributed over this disk of least confusion. The calculation yields an ion current density of 150 kA/cm^2 over the 7-cm^2 spot. Peak focused current densities could be significantly larger. Witness-plate targets located at the focus exhibit multiple layered backspalls through plates of 6.4-mm-thick aluminum (6061-T6), consistent with higher focused current densities than found in the planar-geometry shots.

Fig. 14 — Witness plate damage on Shot 1663 for a 6.4-mm-thick aluminum (6061-T6) plate located at the approximate proton self-focus of a planar pinch-reflex diode
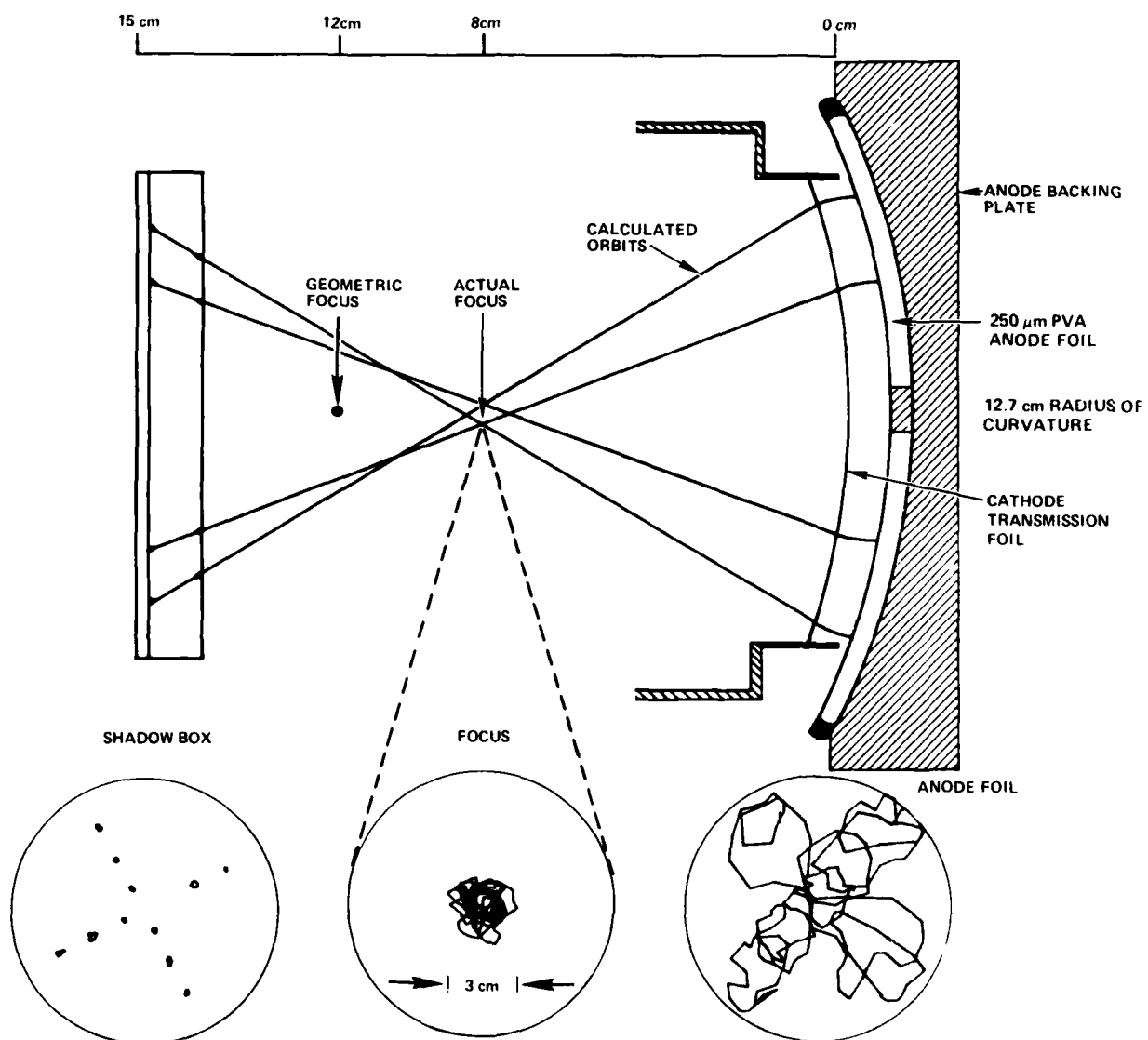
Fig. 15 — Shadowbox geometry for a focusing pinch-reflex diode
and reconstruction of ion trajectories for Shot 1863

28

C. Results from Neutron Measurements

The energy of neutrons from the $D(d,n)^3He$ reaction was determined by the TOF technique. However, this measurement could not be used to determine the deuteron energy (i.e., diode voltage) because the neutron energy is insensitive to the deuteron energy for the d-d reaction at the 175^0 measurement angle. Furthermore, the focusing of deuterons in the diode introduces an uncertainty in the neutron emission angle. Neutron energy determinations are consistent with deuteron energies given by the diode voltage. The measured ion current and diode voltage were used to calculate neutron responses as shown in Fig. 8 (Ref. 23). The shapes of the measured and calculated responses are in good agreement. The low energy tail on the trace at 3.2 m is attributed to scattered neutrons.

For both the planar and focusing diode experiments the measured neutron yields are about 1/3 of yields calculated using the measured ion current and diode voltage corrected for energy loss in the Kimfol. For the planar-diode geometry, the calculated yields are based on the combined thick-target yields for the $D(d,n)^3He$ and $^{12}C(d,n)^{13}N$ reactions at 175^0 as shown in Fig. 7. For the focusing-diode geometry, a broad range of neutron emission angles (140^0-180^0) exists due to the angular spread of the deuterons incident on the CD_2 target. In this case the calculated yield is based on thick-target yields at different angles weighted by an ion-current-density profile[16] determined from numerical simulations. The difference between the measured and calculated neutron yields may be attributed to several factors: 1) The measured ion current may include significant proton or carbon-ion components which contribute very little to the neutron output; 2) Ion energy losses in the region from the anode to the CD_2 target,[30] which have not been taken into account in the neutron-yield calculation, may reduce the ion energy on target and hence the neutron yield; and 3) Enhanced deuteron stopping[31] in the hot dense plasma target may lead to a reduced neutron output, particularly in the focusing diode geometry. A quantitative assessment of the importance of these factors in the present experiments is not possible.

The largest neutron yield at 175^0 was obtained with the planar-diode geometry because the d-d neutron yield peaks at 180^0. For this diode, neutron yields of up to 4.5×10^{11}/sr were measured. At the diode voltage of 1.7 MeV corresponding to this yield, approximately 50% of these neutrons are from the

D(d,n) reaction (see Fig. 7). The corresponding total neutron yield into
4π, corrected for the anisotropy of neutron emission, is 3.7×10^{12} with 50%
from the D(d,n) reaction.

With the focusing-diode geometry, time-integrated neutron yields were
used to determine focused current density by comparing neutron yields from
different area CD_2 targets. For this purpose, the measured neutron output was
scaled to the current measured by the ion Rogowski coil. The fraction of
deuterons incident on targets as small as 0.75 cm^2 was determined by comparing
the neutron yield with the yield measured on 100-cm^2 area targets. On the
0.75 cm^2 area target, the neutron yield was still about 50% greater than that
observed without any CD_2 target. To correct for variations in neutron output
in these measurements due to shot-to-shot variations in voltage and current,
the measured yields were scaled to yields calculated from the measured diode
voltages and ion currents. A deuteron current density of 150 kA/cm^2 at peak
ion voltage was determined from these measurements. If the ion current is
only 1/3 deuterons, as suggested by comparisons between measured and
calculated neutron yields, then the total ion current density may be 2 to 3
times larger than this value.

D. Power Flow Studies

Problems in power flow from the PITHON accelerator to the pinch-reflex
ion diode occurred in the magnetically insulated vacuum transmission line
where a vacuum flow of electrons crossed the feed, reaching the anode before
entering the diode. To inhibit electron leakage, the vacuum biconic and coax
sections were designed with a characteristic impedance gradually decreasing to
a value several times larger than the ion-diode impedance. A parapotential
(Brillouin) flow analysis[32] for this configuration predicts that the entire
electromagnetic-wave energy is transported as boundary current in the
electrodes, with no vacuum electron flow possible. This analysis was found to
be inadequate in these experiments. The diode impedance early in the pulse is
independent of the dielectric anode foil, and is that of a simple pinched-beam
diode with an interelectrode spacing of 8.5 mm, or an impedance of 5 Ω. This
value is very close to the vacuum-feed-coax impedance of 6.5 Ω, and the
Brillouin flow analysis breaks down. Several shots with larger diode gaps
(hence with diode impedance greater than the feed impedance) lead to large-
area current loss in the vacuum feed section and no appreciable power reached

the diode. Analysis of hardware damage for the first experimental
configuration indicated that serious electron losses were occurring near the
abrupt transition between radial and coax lines. A number of polishing,
cleaning, and coating techniques were tried with little improvement to power
flow.

The second experimental session required an extended coax section for
diagnostic access, so an increased electrode spacing was designed to enhance
the magnetic insulation in the coax region. The transition junction from
biconic to coax was designed to be a constant characteristic impedance
of 9.2 Ω . Even so, current loss was again observed beginning 37 ± 11 ns
after current turn-on; a similar delay as in the first session, although the
fractional loss was larger in the second session.

Several vacuum-feed modifications were studied in an attempt to increase
power flow to the diode. These include a "bump" behind the anode foil,
Aerodag versus oil on the coax cathode shank, a smooth conductive covering of
the radial-line anode discontinuities, a smooth shorting of the diode current
monitor, a Krylon coating on the anode side of the vacuum feed, and
enhancement of the cathode tip. The "bump" is a grounded aluminum annulus
typically 1-cm wide mounted behind the plastic anode foil on the backing plate
opposite the cathode tip (see Fig. 4). Its purpose is to lower the early time
Langmuir-Child electron diode impedance and trap the vacuum flow of electrons
emitted in the feed. A sequence of shots taken without the bump, ranging from
2 to 3.5 TW, all showed an early-time current loss between injected (I_0) and
diode (I_D) current monitors (see Fig. 16a). Shots with a smoothly curved
cathode, as in Fig. 4, produced poor pinches without the bump. Shots taken
with a bump did not show the early-time current loss (see Fig. 16b). All low-
power shots taken with the large-area (100 cm^2) cathode and the bump produced
excellent pinches.

At the 4.5-TW level, the bump was not sufficient to ensure good
pinches. Smoothly covering the anode discontinuities with copper tape in the
radial feed and with stainless-steel tubing in the coax feed (bypassing I_D)
produced better pinches and larger PDX signals of greater FWHM. No shots
without this modification produced good pinches at higher power, while 7 out
of 11 shots were excellent with the anode discontinuities covered.
Unfortunately, these modifications eliminated the diode-current measurement,
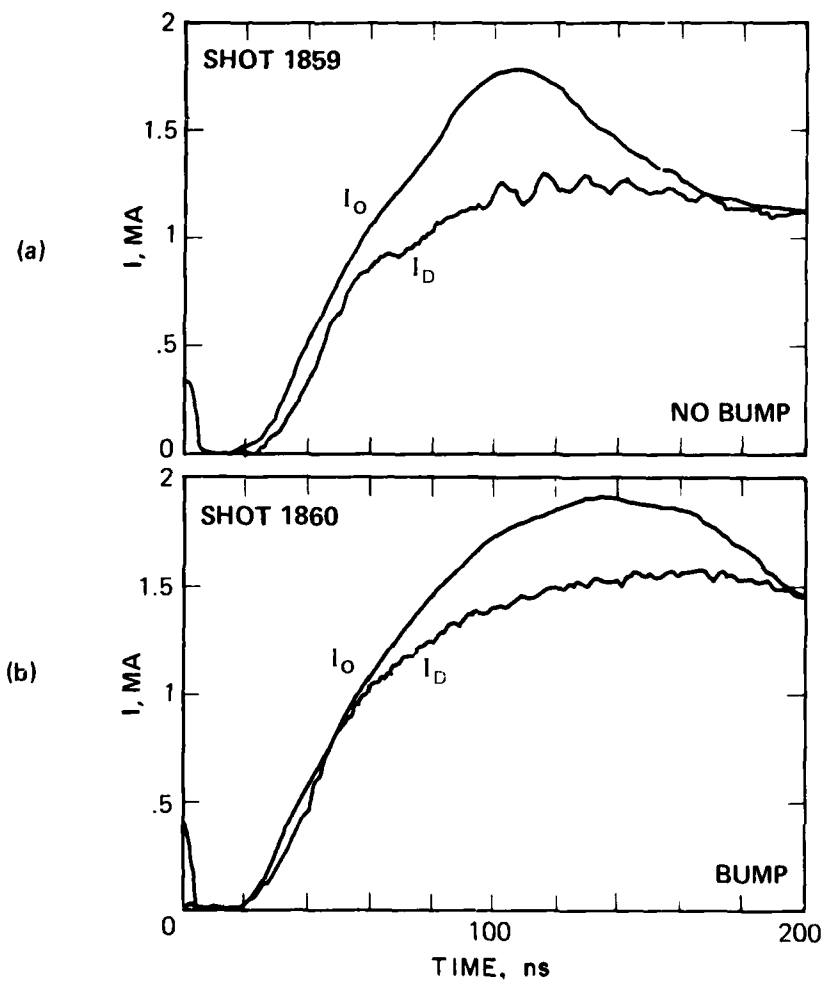
31

Fig. 16 — Comparison of the injected current and diode current (a) on a
shot without the bump (No. 1859) and (b) a shot with the bump (No.
1860). Without the bump, the current loss in the vacuum feed is larger.

32

hence the inductive voltage correction and an upper bound on ion power and energy were unattainable on these shots.

The first experimental session utilized a cathode shank which tapered abruptly from the coax vacuum feed to an extended enhanced cathode tip. Early-time current losses were observed, but the deviations between injected and coupled currents were less than for the hardware shown in Fig. 4. A shot was performed in the second session at 5-TW matched-load power to evaluate cathode-tip-enhancement effects on power flow. A 1-cm-long, 5-mm-wide enhanced lip was welded to the hollow taper cathode, a standard bump was employed, and the diode current monitor engaged. Power loss was again observed, but the pinch was quite good, indicating that this configuration compensates at least in part for the anode-discontinuity effect at high power.

Observations from this study indicate that the modifications to the hardware designed to alleviate the power-flow problem were not effective, suggesting that the geometric transition from radial to coax feed is dominant in power flow over a variation of characteristic impedance. Further, electrode surface is not important, while a well-designed cathode emission tip and a low early-time diode impedance are essential for coupling power from the generator to the diode.

E. Small-Area Diodes

A modification to the diode design was tested to evaluate the performance of smaller-radius diodes with larger ion-current source densities. The hollow taper cathode, shown in Fig. 4, was configured to vary in radius. Shots were taken at 100 cm^2, reported above, and at 30-cm^2 area (see Fig. 4b).

Several small-area diode shots were taken at anode-cathode spacings from 2.6 to 5.6 mm. The small anode-cathode spacings shorted early in the pulse while the large spacings caused the power to dissipate in the lower-impedance vacuum feed. An intermediate spacing of 3.5 mm lead to efficient coupling of the injected energy into the diode without shorting or power loss in the structure. In this case, the diode impedance history was 1. Ω for 50 ns before collapsing (see Fig. 17). A source-area-averaged ion current density of 20 kA/cm^2 at peak power was obtained. The ion-current onset times for this small-area diode were slightly earlier than for the large-area diode as presented in Sec IV A.
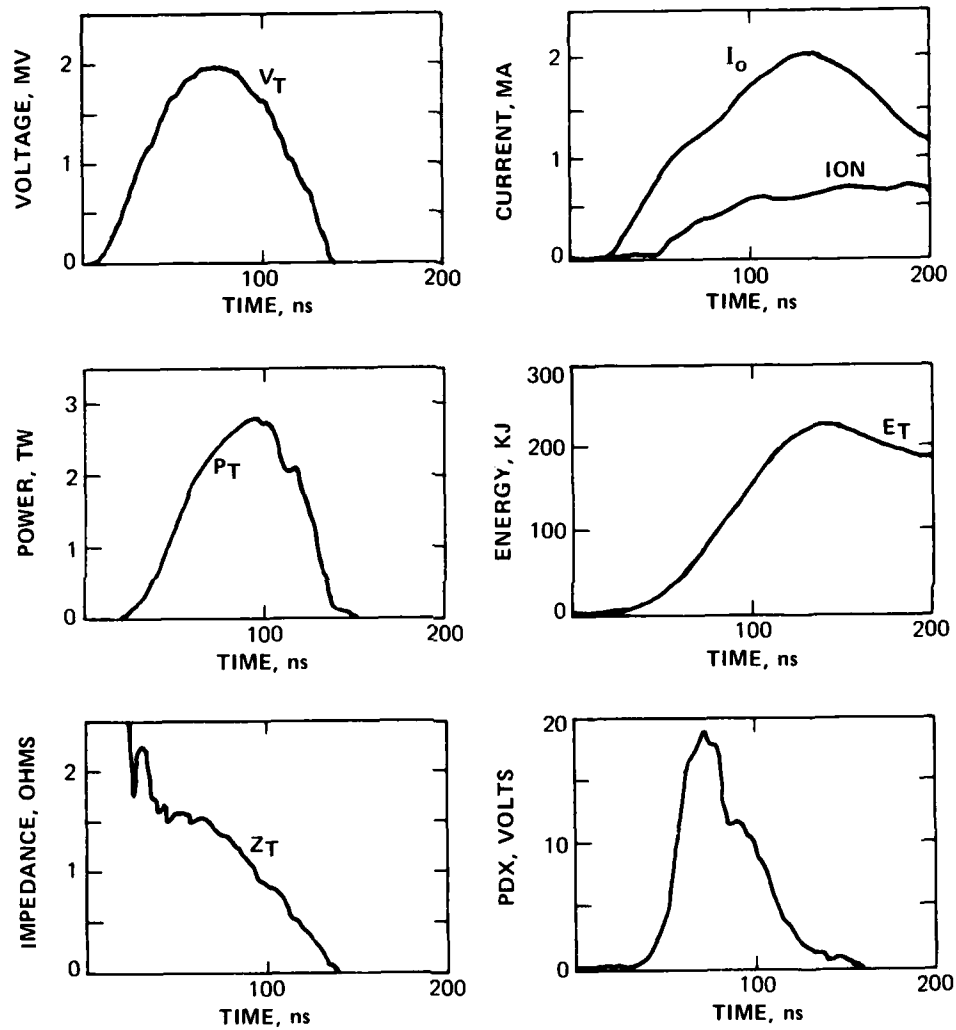
Fig. 17 — Measured waveforms for a 3-TW, 30-cm^2
area pinch-reflex diode shot (No. 1884)

F. Holographic Interferometry

Plasma evolution in the pinch-reflex ion diode was investigated with the holographic interferometry system during the second experimental session. Exposures were made through slots cut in the current return housing of the anode (Fig. 10) to allow a side view of the cathode and anode. The left side of each rectangular slot is defined by the cathode tip, and the right side by the anode foil.

Holograms measured on three different shots are presented in Figs. 18 and 19 and must be compared only in a general way. One can see in Fig. 18 that early in time the plasma density is too small to produce observable fringe shifting. As peak power is approached, significant fringe bending is noticeable near the anode, with smaller effects near the cathode. The greatest effect is near the axis of the diode. One can see in Fig. 19 that later in time significant plasma motion has occurred. The first two holograms (exposures D and E) are for the same shot. For these exposures, optically opaque plasmas have advanced from the electrodes, narrowing the slit through which the laser light can pass to the point that Fraunhofer single-slit diffraction of the light becomes important. Light is clearly visible far outside the borders of the rectangular viewing slits cut in the diode housing. In the slot viewing the diode axis, the plasma has become opaque to the laser light incident during the shot by the time the power pulse has dropped to 40% of its peak value. The adjacent holes have narrowed substantially. A hologram taken after the total collapse of power on another shot, exposure F, shows total opacity everywhere between the electrodes.

Holographic measurements were made on the large-area diode (100 cm^2) for four similar shots at interval spanning most of the power pulse. The timing of the laser-pulse exposures on these shots is shown in Fig. 20. A tracing of each of the four holograms on these shots was made to show the contour corresponding to a line density of 3.2 x $10^{17}/cm^2$, or one fringe shift. These tracings are shown in Fig. 21. The accuracy of the contours is estimated to be ± 0.5 mm of the 3.5 mm anode-cathode gap. Contours for greater fringe shifts were in most cases impossible to extract because large density gradients caused the fringes to run together.

It is clear from the single-fringe-shift reconstructions in Fig. 21 that the plasma fronts expanding from the anode foil and cathode tip are fairly

35
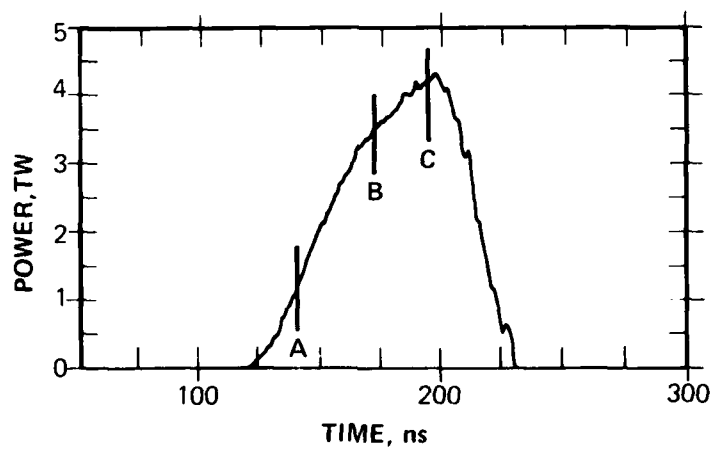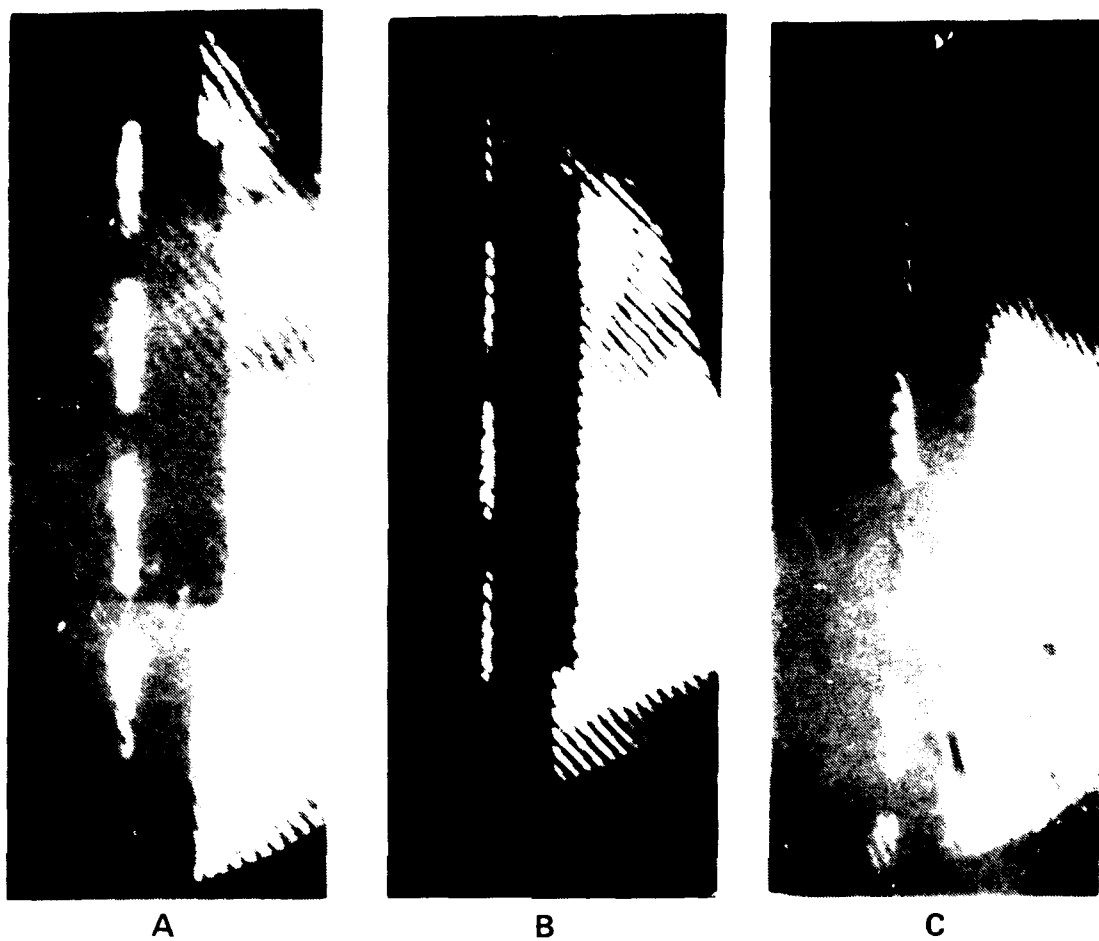
Fig. 18 — Holograms showing plasma formation early in the power pulse for the large-area diode. The timing of the laser-interferometer exposures is indicated by the vertical lines labeled A, B and C on the corresponding power pulse.
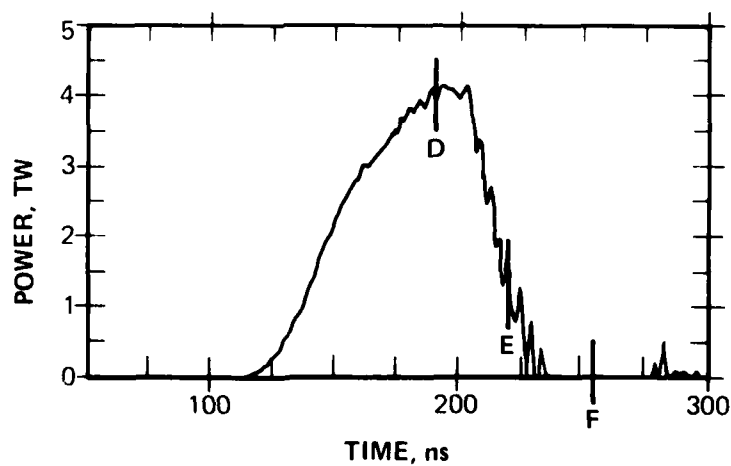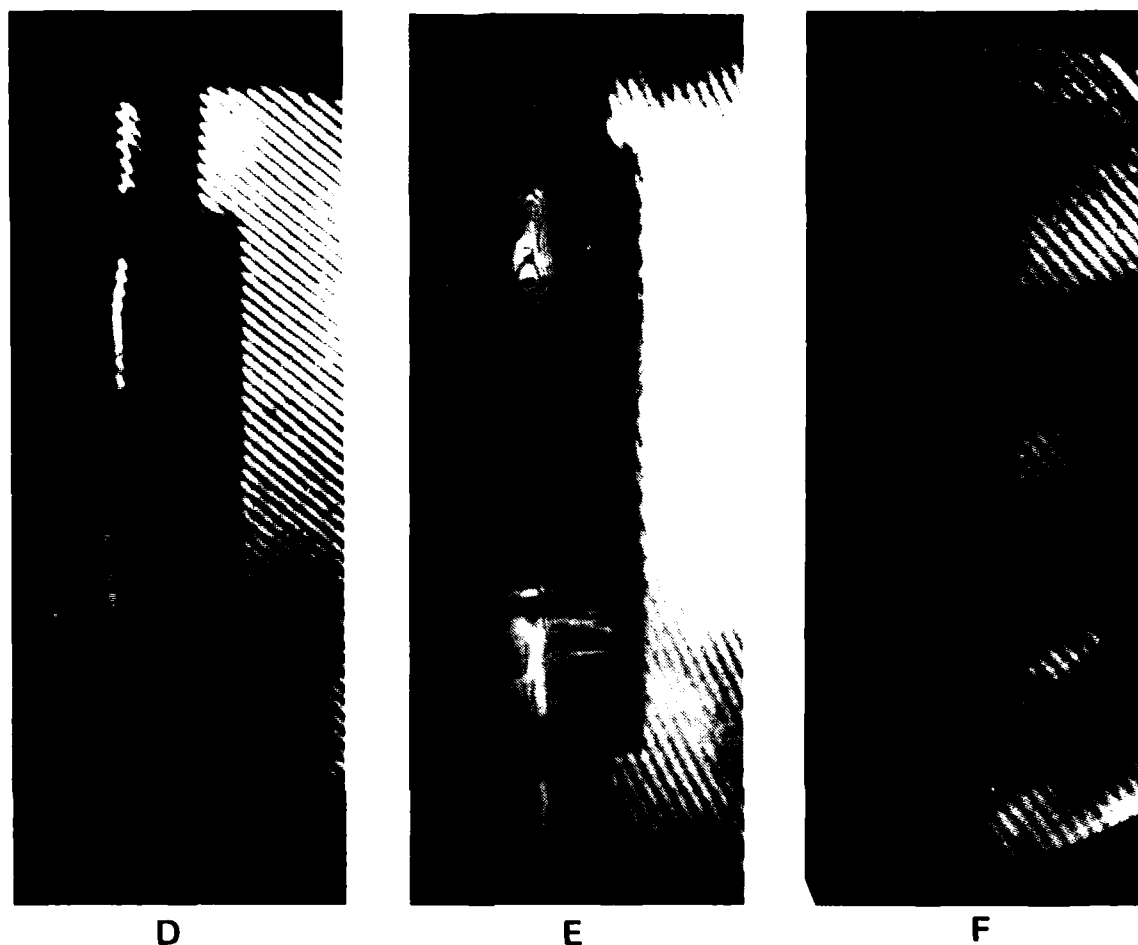
Fig. 19 — Holograms showing late-time plasma evolution for the large-area diode. The timing of the laser interferometer exposures is indicated by the vertical lines labeled D, E and F on the corresponding power pulse.

37

Fig. 20 — Timing of the laser-interferometer exposures relative to the power pulse on four different pinch-reflex diode shots. The vertical lines labeled A, B, C and D indicate the times at which the exposures are recorded on each shot.

38

(a) Shot 1873

(b) Shot 1875

(c) Shot 1878
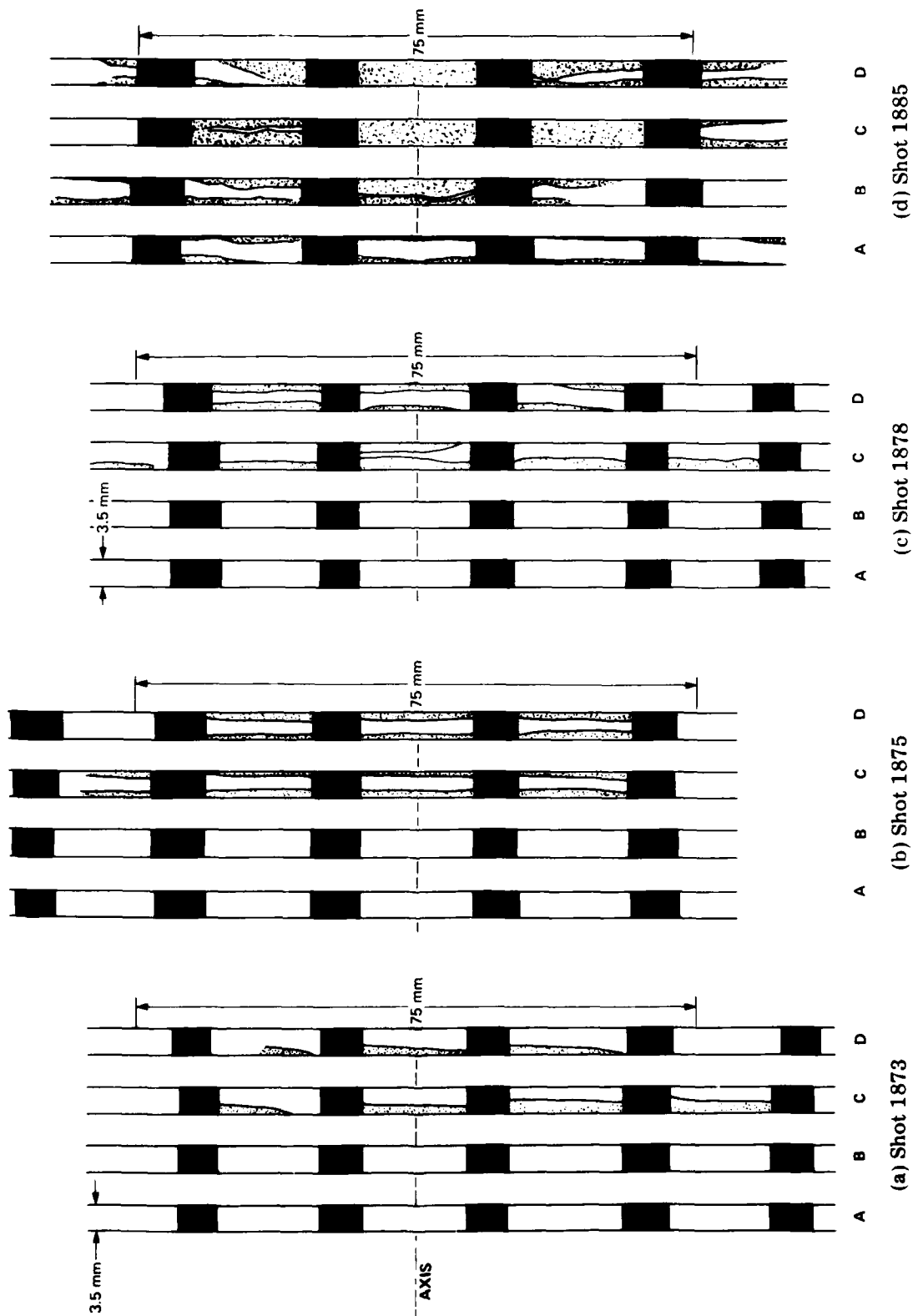
(d) Shot 1885

Fig. 21 — Single-fringe-shift reconstructions corresponding to the holograms measured on (a) Shot 1873, (b) Shot 1875, (c) Shot 1878 and (d) Shot 1885. The shaded regions indicate plasma line densities greater than $3.2 \times 10^{17}/cm^2$.

regular with gentle surface fluctuations and are not, in general, cylindrically symmetric. The absence of sharp plasma protrusions argues for a reasonable beam emittence, although a smoother and more regular plasma surface is required for high-focus-quality beam development. The important points to notice are that the plasmas expand from the boundary surface as the power pulse approaches its peak, that they are reasonably uniform and approach one another at increasing velocities, and that the center velocity appears greater than the larger-radius plasma motions.

The contours of Shot 1885 (Fig. 21d), showing the plasma behavior during the power collapse, indicate a considerable change between the first and second frames, both of which were taken near peak power. The plasma closure velocity implied on axis is 27 cm/μs; off axis at a radius of 3 cm the velocity is 7 cm/μs between frames A and B, and 10 cm/μs between frames B and C. The line density off axis is seen to decrease in the last frame, allowing light to again pass through holes that were formerly opaque. This phenomenon may be due to the anode plasma being compressed by magnetic pressure. Alternatively, the anode and cathode plasmas may never have met in the earlier frames, but the opacity there may have been caused by surface fluctuations or ripples that blocked the laser line-of-sight.

The plausibility of the magnetic-pressure mechanism can be determined by calculating the time required for the plasma pressure to be overcome by the rising magnetic pressure in the diode gap. Energy is deposited into the anode plasma continuously throughout the pulse, increasing the particle kinetic energy. The decreasing diode impedance means that early in time the current (and hence magnetic field) is low so $nkT \gg B^2/2\mu$. Later the impedance decreases and the magnetic pressure increases more quickly than the plasma thermal energy. Rough parameters appropriate to the diode at the time of impedance collapse could be 2 MA flowing within a 3-cm radius, a plasma density of about $10^{18}/cm^3$ of CH_2 components, and a temperature of 5 eV. The magnetic pressure for these values is 67 MPa while the thermal pressure is 0.75 MPa, clearly much smaller. These yield an acceleration of 120 cm/μs^2 and a time of 16 ns for anode and cathode plasmas to each move 1.5 mm. This value is comparable to the observed 10-ns time scale of plasma motion across the diode. While plasma surface fluctuations cannot be ruled out as the source of diode opacity after peak power, the most likely explanation is the

ejection of plasma from the diode into the hollow cathode cavity and back to the anode location by magnetic pressure from the diode short circuit.

In addition to the 3-TW, 100-cm^2 diode shots, several shots at 2 to 2.5-TW diode power with a small-area (30 cm^2) diode were holographically monitored (Fig. 22). On Shot 1886 (Fig. 22a) interferograms of the diode during the ascent to peak power were recorded, indicating little plasma motion before peak power and with noticeable motion within a radius of 3 cm during the last two frames at peak power. The closure velocity on axis between the last two frames is 21 cm/μs.

On two other small-diameter shots, arcs occurred in different parts of the feed early in time. On Shot 1879, the arc formed well upstream from the diode in the coaxial vacuum feed. A perturbation in the reference fringes on one side of the diode is the only indication of the event (Fig. 22b). On Shot 1880, the arc was in the diode, resulting from too small an electrode separation. The diode was opaque to laser light even in the first hologram and hence density contour mapping was not possible.

V. SUMMARY OF RESULTS

In this paper, we have presented recent technological advances in intense pulsed ion-beam development. The pinch-reflex diode has been successfully scaled up to multiterawatt operation on the PITHON accelerator. Pulsed proton and deuteron beams have been produced in both planar and spherically focusing geometries with 1.0-MA of 1.8-MeV light ions measured at a peak power of 1.8 TW yielding a 130-kJ light ion beam in 100 ns.

Focusing of intense ion beams by electrode shaping and by self-magnetic field deflection has been shown at large radii to follow simple theoretical modeling with several corroborating diagnostics. Spherical electrode shaping served to compress the ion beam from an 11-cm-diam anode surface to a 3-cm-diam focal spot located, due to magnetic bending, inside the geometric focus. Small-area diode tests at lower power demonstrated that impedance lifetime is not a problem at higher source-current-density levels. Further, these results suggest that a smaller-area pinch-reflex diode of higher power density may be suitable for injection into a plasma transport channel.

The most serious problem encountered in these experiments was independent

41
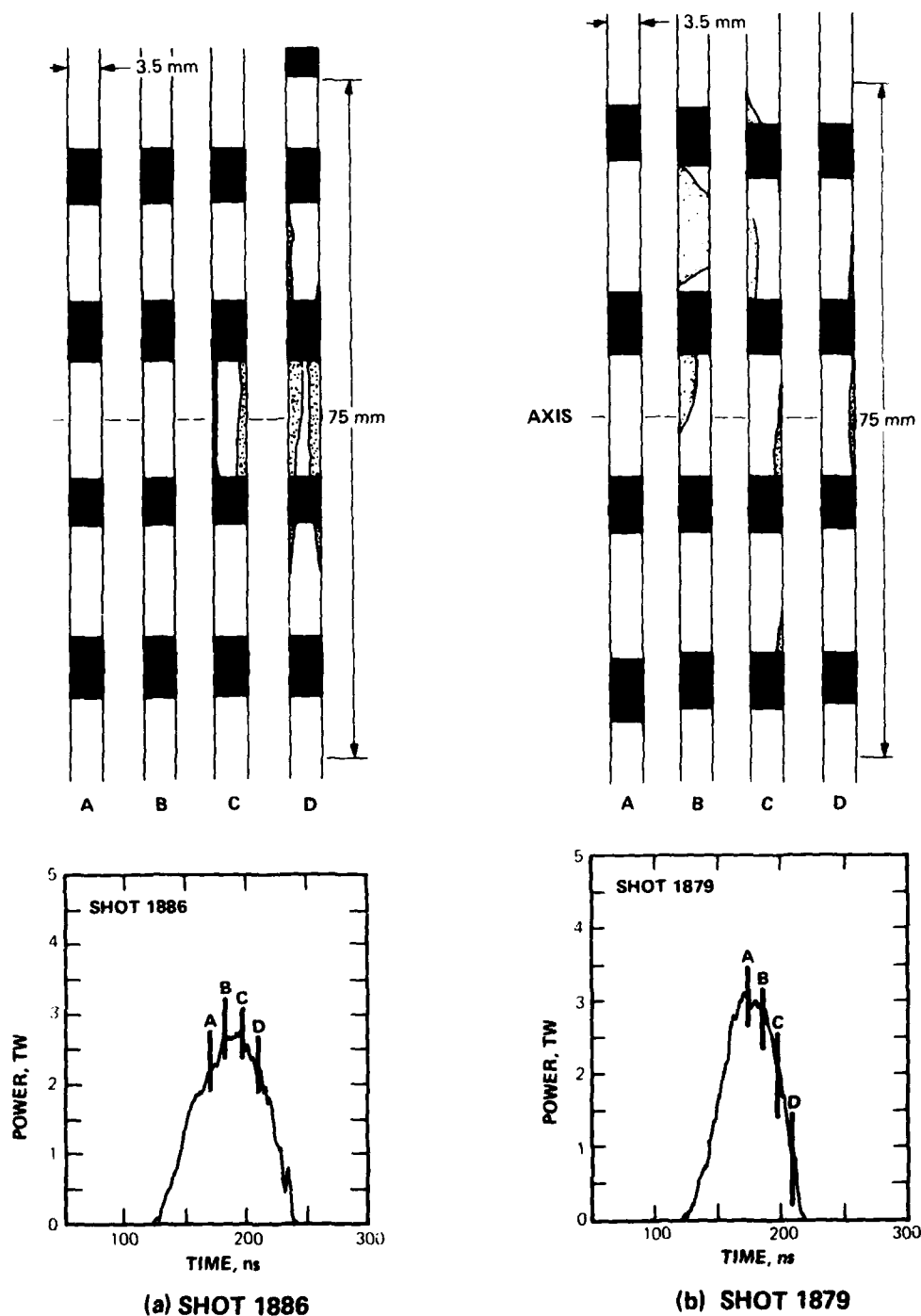
Fig. 22 — Single-fringe-shift reconstructions for (a) Shot 1886 and (b) Shot 1879. The timing of the laser interferometer exposures is indicated by the vertical li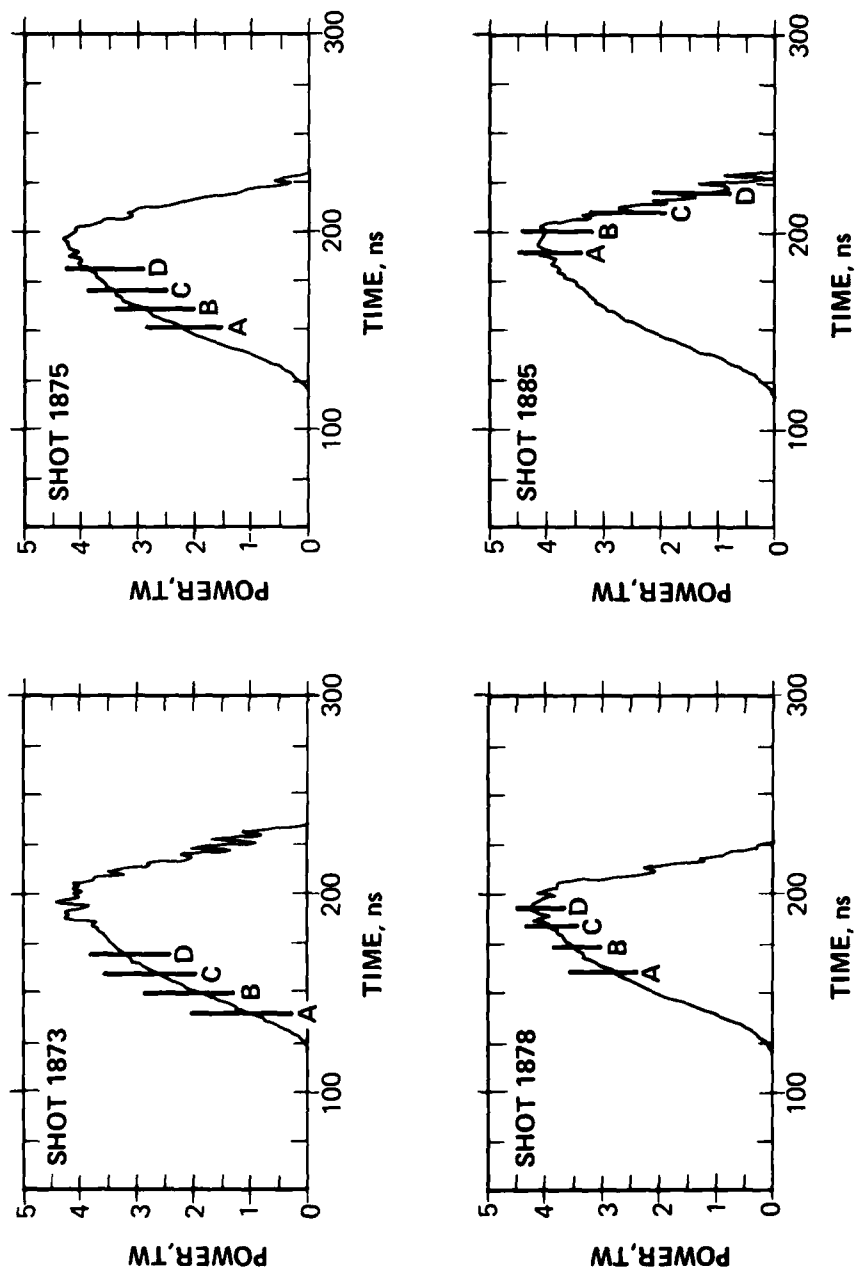nes labeled A, B, C and D on the corresponding power pulses. The shaded regions indicate plasma line densities greater than $3.2 \times 10^{17}/cm^2$.

42

of the pinch-reflex diode but concerned the coupling of power from the accelerator interface through the vacuum feed structure to the diode. These losses were found to be geometric, that is, independent of electrode surface, and occurred principally between the biconic-to-coax transition and the diode. Reducing the early-time diode impedance, smoothing the vacuum feed of resonant grooves, and enhancing the cathode emission tip all served to increase the power flow to the diode.

Beam diagnostics were developed to survive the harsh bremsstrahlung and impulse environment of a 3-TW pinch-reflex diode. Measurements of nuclear-reaction products provided total ion yields and pulse-shape evaluations. Total beam Rogowski coil monitors were developed to perform through the time of peak power. The shadowbox technique provided beam-focus location and local-beam divergence.

A first study of the spatial evolution of the anode and cathode plasmas in a 3-TW pinch-reflex diode was performed on multiple shots spanning the power pulse. Surfaces at constant line density ($3 \times 10^{17}/cm^2$) are observed to expand from the electrodes at times approaching peak power in fairly uniform though nonsymmetric profiles and accelerate toward one another. After peak power, significant anode-plasma surface fluctuations and a high velocity (up to 30 cm/μs) axial plume were observed. During the power pulse collapse a high density ($n > 10^{18}/cm^3$) plasma bridges the anode-cathode gap over the central 7.5-cm diameter. On some shots the high density plasma is later seen to open suggesting magnetic plasma confinement. The knowledge of the anode and cathode shapes at peak power suggests that further research into the formation of more uniform plasmas is necessary for development of a highly focused ion diode. The measured evolution of the shapes of the anode and cathode plasmas is the information required to design a first iteration modification to the simple spherically focusing anode.

REFERENCES

1. See for example: G. Yonas, 4th ANS Topical Meeting on Technology of Controlled Nuclear Fusion, October 14-17, 1980, Valley Forge, Pennsylvania; and S. Humphries, Jr., SAND 80-0402, Sandia Laboratories, 1980.

2. G. Cooperstein, S.A. Goldstein, D. Mosher, R.J. Barker, J.R. Boller, D.G. Colombant, A. Drobot, R.A. Meger, W.F. Oliphant, P.F. Ottinger, F.L. Sandel, S.J. Stephanakis, and F.C. Young, in Laser Interaction and Related Plasma Phenomena, H. Schwarz, H. Hora, M. Lubin and B. Yaakobi, Editors (Plenum, New York, 1981), Vol. 5, p. 105.

3. V.M. Bystritsky and A.N. Didenko, Uspekhi Fizicheskikh Nauk 132, 91 (1980).

4. J.W. Shearer, Nucl. Fusion 15, 952 (1975).

5. M.J. Clauser, Phys Rev. Lett. 35, 849 (1975).

6. R.O. Bangerter and D.J. Meeker, in Proc. 2nd Int. Topical Conf. on High Power Electron and Ion Beam Res. and Tech.,J.A. Nation and R.N. Sudan, Editors, (Cornell University, Ithaca, New York, 1977), p. 183.

7. J. Maenchen, L. Wiley, S. Humphries, Jr., E. Peleg, R.N. Sudan, and D.A. Hammer, Phys. Fluids 22, 555 (1979).

8. S.A. Goldstein, G. Cooperstein, Roswell Lee, D. Mosher and S.J. Stephanakis, Phys. Rev. Lett. 40, 1504 (1978).

9. S. Humphries, Jr., J. Appl. Phys. 51, 1876 (1980).

10. P.F. Ottinger, D. Mosher, and S.A. Goldstein, Phys. Fluids 23, 909 (1980).

11. D. Mosher, G. Cooperstein, S.J. Stephankis, S.A. Goldstein, D.G. Colombant, and Roswell Lee, Report No. 3658, Naval Research Laboratory, 1977.

12. G. Frazier, in Proc. NSWC Pulse Power Systems Workshop (Cornell University, Ithaca, New York, Sept. 1976).

13. D. Mosher, D. G. Colombant, and S.A. Goldstein, Comments Plasma Phys. 6, 101 (1981).

14. D. Mosher, Bull. Am. Phys. Soc., Ser. II, 25, 900 (1980).

15. D.G. Pellinen, Marco S. DiCapua, S.E. Sampayan, H. Gerbracht, and M. Wang, Rev. Sci. Instrum. 51, 1535 (1980).

16. A. Drobot, Roswell Lee, S.A. Goldstein, and G. Cooperstein, IEEE Conf. Record Abstracts, 1979 IEEE Int. Conf. on Plasma Sci. (Montreal, Canada, June 4-6, 1979), IEEE No. 79CH1410-0 NPS, p. 78.

17. F.C. Young, W.F. Oliphant, S.J. Stephanakis, and A.R. Knudson, IEEE Trans. Plasma Sci. PS-9, 24 (1981).

18. F.C. Young, IEEE Trans. Nucl. Sci. NS-22, 718 (1975).

19. H. Liskien and A. Paulsen, Nuclear Data Tables 11, 569 (1973).

20. H.W. Lefevre, C.A. Burke, and R.M. Bahnsen, Report No. RLO-1925-44, University of Oregon, 1971.

21. H.H. Andersen and J.F. Ziegler, Stopping Powers and Ranges in all Elements, (Pergamon Press, New York, 1977), Vol. 3.

22. J.G. Pronko, T.R. Fisher, and L.F. Chase, Nucl. Instr. and Meth. 163, 227 (1979).

23. F.C. Young, D. Mosher, S.J. Stephankis, S.A. Goldstein, and D. Hinshelwood, Memo Report No. 3823, Naval Research Laboratory, 1978.

24. K. Triebes and R. Huff, Bull. Am. Phys. Soc., Sec. II, 19, 976 (1974).

25. D. Mosher, G. Cooperstein, and S.A. Goldstein in Technical Digest of Conf. on Inertial Confinement Fusion (San Diego, California, February 26-28, 1980), IEEE No. 80CH1536-2 QEA, p. 104.

26. A.E. Blaugrund, G. Cooperstein and S.A. Goldstein in Proc. Int. Topical Conf. on Electron Beam Res. and Tech. G. Yonas, Editor, SAND76-5122, (Albuquerque, New Mexico, Feb., 1976) Vol. I, p. 233.

27. R.D. Genuario and V.L. Bailey, Appl. Phys. Lett. 33, 694 (1978).

28. J.C. Martin "Nanosecond Pulse Techniques," SSWA/JCM/704/49, Internal Report, AWRE, Aldermaston, England, 1970.

29. H.W. Koch and J.W. Motz, Rev. Mod. Phys. 31, 4 (1959).

30. F.C. Young, S.J. Stephanakis, G. Cooperstein, D. Mosher, F.L. Sandel, P.G. Blauner and S.A. Goldstein, Naval Research Laboratory Report 4322, 1980.

31. E. Nardi, E. Peleg and Z. Zinamon, Appl. Phys. Lett. 39, 46 (1981).

32. J. Creedon, J. Appl. Phys. 48, 2946 (1975).

AUGUST 1981

Director
Defense Intelligence Agency
Washington, DC 20301

Attn: DTICI Robert I. Rubenstein   1 copy

Defense Advanced Research Project Agency
1400 Wilson Blvd.
Arlington, VA 22209
Attn: J. Bayless   1 copy

Director
Defense Nuclear Agency
Washington, DC 20305

Attn: FCPR   1 copy
      STVL   1 copy
      TISI Archives   1 copy
      TITL Tech. Library   3 copies
      J. Z. Farber (RAEV)   1 copy
      R. L. Gullickson (RAEV)   1 copy

Defense Technical Information Center
Cameron Station
5010 Duke Street
Alexandria, VA 22314

Attn: T. C.   12 copies

Under Sec'y of Defense for RSCH and ENGRG
Department of Defense
Washington, DC 20301

Attn: S&SS(OS)   1 copy

Chief
Livermore Division Fld Command DNA
Lawrence National Laboratory
P. O. Box 808
Livermore, CA 94550

Attn: FCPRL   1 copy

National Technical Information Service
U.S. Department of Commerce
5285 Port Royal Road
Springfield, VA 22161   24 copies

Commander
BMD System Command
P. O. Box 1500
Huntsville, AL 35807

Attn: SSC-TEN   1 copy

DEP Chief of Staff for RSCH DEV & ACQ
Department of the Army
Washington, DC 20310

Attn: DAMA-CSM-N   1 copy

Commander
Harry Diamond Laboratories
2800 Powder Mill Road
Adelphi, MD 20783
(CNWDI-INNER ENVELOPE: ATTN: DELHD-RBH)

Attn: DELHD-NP   1 copy
      DELHD-RCC J. A. Rosado   1 copy
      DRXDO-RBH P. A. Caldwell   1 copy

      DRXDO-TI   Tech. Lib.   1 copy
      S. Graybill   1 copy

Commander
Picatinny Arsenal
Dover, NJ 07801

Attn: SMUPA ND-N-E   1 copy

U. S. Air Force Office of Scientific Research
Physics Directorate
Bolling A.F.B., DC 20332

Attn: A. K. Hyder   1 copy
      M. A. Stroscio   1 copy

Commander
U. S. Army Missile Command
Redstone Arsenal, AK 35809

Attn: Redstone Scientific Information CTR
      DRCPM-PM-PE-EA   1 copy

Commander
U. S. Army Nuclear Agency
7500 Backlick Road
Building 2073
Springfield, VA 22150

Attn: ATCN-W   1 copy

Commander
U. S. Army Test and Evaluation COMD
Aberdeen Proving Ground, MD 21005

Attn: DRSTE-EL   1 copy

Commander
Naval Electronic Systems CMD HQS
Washington, DC 20360

Attn: Code 5032   1 copy

Commanding Officer
Naval Intelligence Support Center
4301 Suitland Road - Building 5
Washington, DC 20390

Attn: NISC-45   1 copy

Naval Research Laboratory
  Addressee: Attn: Name/Code
  Code 2628 - TIC-Distribution   25 copies
  Code 4040 - J. Boris   1 copy
  Code 6682 - D. Nagel   1 copy
  Code 4700 - T. Coffey   26 copies
  Code 4707 - J. Davis   1 copy
  Code 4730 - S. Bodner   1 copy
  Code 4740 - V. Granatstein   1 copy
  Code 4760 - B. Robson   1 copy
  Code 4761 - C. Kapetanakos   1 copy
  Code 4770 - Branch Head   10 copies
  Code 4770 - F. Young   1 copy
  Code 4770 - S. Stephanakis   1 copy
  Code 4771 - D. Mosher   10 copies
  Code 4773 - G. Cooperstein   10 copies
  Code 4790 - D. Colombant   1 copy
  Code 4790 - I. Haber   1 copy
  Code 4790 - M. Lampe   1 copy
On-Site Contractors:
  Code 4770 - R. Barker (Jaycor)   1 copy
  Code 4770 - S. Goldstein (Jaycor)   1 copy
  Code 4770 - R. Meger (Jaycor)   1 copy
  Code 4770 - P. Ottinger (Jaycor)   1 copy
  Code 4770 - F. Sandel (Jaycor)   1 copy
  Code 4790 - A. Drobot (SAI)   1 copy

Officer-in-Charge
Naval Surface Weapons Center
White Oak, Silver Spring, MD 20910

Attn: Code WR43   1 copy
       Code WA501 - Navy Nuc Prgms Off 1 copy

Chief of Naval Operations
Navy Department
Washington, DC 20350

Attn: R. A. Blaise 604C4   1 copy

Commander
Naval Weapons Center
China Lake, CA 93555

Attn: Code 533 Tech Lib.   1 copy

AF Weapons Laboratory, AFSC
Kirtland AFB, NM 87117

Attn: CA   1 copy
       ELC   1 copy
       NT   1 copy
       SUL   1 copy
       DYP   1 copy
       J. Darrah   1 copy
       W.L. Baker   1 copy
HQ USAF/RD
Washington, DC 20330

Attn: RDQSM   1 copy

Director
Joint Strat TGT Planning Staff JCS
OFFUTT AFB
Omaha, NB 68113
Attn: JSAS   1 copy

SAMSO/DY
Post Office Box 92960
Worldway Postal Center
Los Angeles, CA 90009
(Technology)

Attn: DYS   1 copy

SAMSO/IN
Post Office Box 92960
Worldway Postal Center
Los Angeles, CA 90009

Attn: IND MAJ D. S. Muskin   1 copy

SAMSO/MN
Norton AFB, CA 92409
(Minuteman)

Attn: MNNH   1 copy

SAMSO/SK
Post Office Box 92960
Worldway Postal Center
Los Angeles, CA 90009
(Space Comm Systems)

Attn: SKF P. H. Stadler   1 copy

U. S. Department of Energy
Division of Inertial Fusion
Washington, DC 20545

Attn: G. Canavan   1 copy
       T. F. Godlove   1 copy
       S. L. Kahalas   1 copy
       R. L. Schriever   1 copy

U.S. Department of Energy
P.O. Box 62
Oak Ridge, TN 37830   50 copies

Argonne National Laboratory
9700 South Cass Avenue
Argonne, Illinois 60439

Attn: G. R. Magelssen   1 copy
       R. J. Martin   1 copy

Brookhaven National Laboratory
Upton, NY 11973

Attn: A.F. Maschke   1 copy

Lawrence Berkley Laboratory
Berkeley, CA 94720

Attn: D. Keefe   1 copy

Lawrence Livermore National Laboratory
P. O. Box 808
Livermore, CA 94550

Attn:	L-18	1 copy
	L-153	1 copy
	R. J. Briggs	1 copy
	E. P. Lee	1 copy
	J. H. Nuckolls	1 copy
	S. S. Yu	1 copy
	Tech Info Dept. L-3	1 copy
	D.J. Meeker	1 copy
	A.B. Langdon	1 copy
	E. Teller	1 copy
	D.S. Prono	1 copy

Los Alamos National Laboratory
P. O. Box 1663
Los Alamos, NM 87545

Attn:	D. B. Henderson	1 copy
	R. B. Perkins	1 copy
	L. E. Thode	1 copy
	C. Barnes	1 copy
	D. Forslund	1 copy
	R.O. Bangerter	1 copy
	W.P. Gula	1 copy

National Science Foundation
Mail Stop 19
Washington, DC 20550

| Attn: D. Berley | 1 copy |

Sandia National Laboratories
P. O. Box 5800
Albuquerque, NM 87185

Attn:

J. R. Freeman / 4241	1 copy
S. Humphries / 4253	1 copy
D. J. Johnson / 4244	1 copy
G. W. Kuswa / 4240	1 copy
P. A. Miller / 4244	1 copy
J. P. Vandevender / 4252	1 copy
G. Yonas / 4200	1 copy
Doc Con for 3141 Sandia RPT Coll	1 copy
J.N. Olsen / 4244	1 copy
G.A. Allshouse / 4247	1 copy
T.A. Mehlhorn / 4247	1 copy
M.M. Widner / 4247	1 copy
T.P. Wright / 4241	1 copy
J.P. Quintenz / 4241	1 copy
P.L. Mix / 4242	1 copy
C.W. Mendel /4244	1 copy
A.V. Farnsworth / 4247	1 copy
M.A. Sweeney / 4247	1 copy
D.B. Seidel / 4241	1 copy

AVCO Research and Systems Group
201 Lowell Street
Wilmington, MA 01887

| Attn: Research Lib. A830 Rm. 7201 | 1 copy |

BDM Corporation, The
795 Jones Branch Drive
McLean, VA 22101

| Attn: Tech Lib. | 1 copy |

Bechtel Group, Inc.
P.O. Box 3965
San Francisco, CA 94119

| Attn: W. O. Allen | 1 copy |

Boeing Company, The
P. O. Box 3707
Seattle, WA 98124

| Attn: Aerospace Library | 1 copy |

Cornell University
Ithaca, NY 14850

Attn:	D. A. Hammer	1 copy
	R. N. Sudan	1 copy
	J. Maenchen	1 copy
	J.B. Greenley	1 copy
	C.B. Wharton	1 copy

The Dikewood Corporation
1613 University Blvd., NE
Alburquerque, NM 87102

| Attn: L. Wayne Davis | 1 copy |

EG&G, Inc.
Albuquerque Division
P. O. Box 10218
Albuquerque, NM 87114

| Attn: Technical Library | 1 copy |

Electric Power Research Institute
3412 Hillview Avenue
P.O. Box 10412
Palo Alto, CA 94303

| Attn: K.W. Billman | 1 copy |

Ford Aerospace & Communications Operations
Ford & Jamboree Roads
Newport Beach, CA 92663
(Formerly Aeronutronic Ford Corporation)

| Attn: Tech Info Section | 1 copy |

General Electric Company
Space Division
Valley Forge Space Center
Goddard Blvd., King of Prussia
P. O. Box 8555
Philadelphia, PA 19101

| Attn: J. C. Penden VFSC, Rm. 4230M | 1 copy |

General Electric Company
Tempo-Center for Advanced Studies
816 State Street (P. O. Drawer QQ)
Santa Barbara, CA 93102

| Attn: DASIAC | 1 copy |

Grumman Aerospace Corporation
Bethpage, NY 11714

Attn: P. Suh   1 copy

Institute for Defense Analyses
400 Army-Navy Drive
Arlington, VA 22202

Attn: IDA Librarian R S. Smith   1 copy

Ion Physics Corporation
South Beford Street
Burlington, MA 01803

Attn: H. Milde   1 copy

IRT Corporation
P. O. Box 81087
San Diego, CA 92138

Attn: R. L. Mertz   1 copy

JAYCOR, Inc.
205 S. Whiting Street
Alexandria, VA 22304

Attn: E. Alcaraz   1 copy
       J. Guillory   1 copy
       R. Hubbard   1 copy
       R. Sullivan   1 copy
       D. A. Tidman   1 copy

JAYCOR, Inc.
11011 Torreyana Road
San Diego, CA 92121

Attn: E. Wenaas   1 copy
       S.S. Wang   1 copy

Kaman Science Corporation
P. O. Box 7463
Colorado Springs, CO 80933

Attn: A. P. Bridges   1 copy
       D. H. Bryce   1 copy
       J. R. Hoffman   1 copy
       W. E. Ware   1 copy

Lockheed Missiles and Space Co., Inc.
3251 Hanover Street
Palo Alto, CA 94304

Attn: L. F. Chase   1 copy

Massachusetts Institute of Technology
Cambridge, MA. 02139

Attn: R.C. Davidson   1 copy
       G. Bekefi   1 copy
       D. Hinshelwood   1 copy

Maxwell Laboratories, Inc.
9244 Balboa Avenue
San Diego, CA 92123

Attn: R. W. Clark   1 copy
       A. C. Kolb   1 copy
       P. Korn   1 copy
       A. R. Miller   1 copy
       J. Pearlman   1 copy
       J. Shannon   1 copy

McDonnell Douglas Corporation
5301 Bolsa Avenue
Huntington Beach, CA 92647

Attn: S. Schneider   1 copy

Mission Research Corporation
1400 San Mateo Blvd. SE
Albuquerque, NM 87108

Attn: B. B. Godfrey   1 copy

Mission Research Corporation-San Diego
P. O. Box 1209
LaJolla, CA 92038

Attn: V.A.J. Van Lint   1 copy

Mission Research Corporation
735 State Street
Santa Barbara, CA 93101

Attn: W. C. Hart   1 copy
       C. L. Longmire   1 copy

Northrop Corporation
Electronic Division
2301 West 120th Street
Hawthorne, CA 90250

Attn: V. R. DeMartino   1 copy

Northrop Corporation
Northrop Research and Technology Ctr.
3401 West Broadway
Hawthorne, CA 90205   1 copy

Physical Dynamics
P.O. Box 556
La Jolla, CA 92037

Attn: S. Jorna   1 copy

Physics International Co.
2700 Merced Street
San Leandro, CA 94577

Attn: J. Benford   1 copy
       B. Bernstein   1 copy
       G. Frazier   1 copy
       E. B. Goldman   1 copy
       R. Huff   1 copy
       A. J. Toepfer   1 copy
       G. Dahlbacka   1 copy

Power Conversion Technology, Inc. 1158 Sorrento Valley Road San Deigo, CA 92121		Systems, Science and Software, Inc. P. O. Box 1620 LaJolla, CA 92038	
Attn: V. Fargo D.A. Phelps	1 copy 1 copy	Attn: A. R. Wilson	1 copy
Princeton Plasma Physics Laboratory James Forrestal Campus P.O. Box 451 Princeton, N.J. 03540		Texas Tech University P. O. Box 5404 North College Station Lubbock, TX 79417	
		Attn: T. L. Simpson M. Kristiansen	1 copy 1 copy
Attn: R. Kulsrud	1 copy		
Pulse Sciences, Inc. 1615 Broadway, Suite 610 Oakland, CA 94612		TRW Defense and Space Sys Group One Space Park Redondo Beach, CA 90278	
Attn: I. Smith P. Spence S. Putnam	1 copy 1 copy 1 copy	Attn: Tech Info Center/S-1930 Z.G.T. Guiragossian D. Arnush	1 copy 1 copy 1 copy
R&D Associates P. O. Box 9695 Marina Del Rey, CA 90291		University of California Dept. of Physics La Jolla, CA 92037	
Attn: W. R. Graham, Jr. M. Grover C. MacDonald E. Martinelli	1 copy 1 copy 1 copy 1 copy	Attn: K. Brueckner W.B. Thompson	1 copy 1 copy
		University of California Boelter Hall 7731 Los Angeles, CA 90024	
R&D Associates Suite 500 1401 Wilson Blvd. Arlington, VA 22209		Attn: F.F. Chen	1 copy
Attn: P. J. Turchi	1 copy	University of California Irvine, CA 92717	
Science Applications, Inc. P. O. Box 2351 LaJolla, CA 92038		Attn: G. Benford N. Rostoker S. Robertson A. Fisher	1 copy 1 copy 1 copy 1 copy
Attn: J. Robert Beyster	1 copy	University of Illinois Urbana, IL 61801	
Spire Corporation P. O. Box D Bedford, MA 01730		Attn: G. H. Miley J. T. Verdeyen	1 copy 1 copy
Attn: R. G. Little	1 copy	University of Rochester Laboratory of Laser Energetics River Station, Hopeman 110 Rochester, NY 14627	
SRI International 333 Ravenswood Avenue Menlo Park, CA 94025		Attn: Director	1 copy
Attn: S. Odairiki R.J. Vidmar	1 copy 1 copy	University of Scranton Dept. of Physics Scranton, PA 18510	
Stanford University SLAC P. O. Box 4349 Stanford, CA 94305		Attn: F. Murray	1 copy
Attn: W. B. Herrmannsfeldt	1 copy		

Univ. of Washington
Dept. of Nuclear Engineering
BF-10
Seattle, WA 98115

Attn: F. Ribe   1 copy

Univ. of Wisconsin
Dept. of Nuclear Engineering
1500 Johnson Drive
Madison, WI 53706

Attn: G.A. Moses   1 copy
       G.L. Kulcinski   1 copy

Vought Corporation
Michigan Division
38111 Van Dyke Road
Sterling Heights, MI 48077
(Formerly LTV Aerospace Corp)

Attn: Tech Lib   1 copy

Westinghouse Electric Corporation
Research and Development Center
1310 Beulah Road
Pittsburgh, PA 15235

Attn: M.D. Nahemow   1 copy

Atomic Weapons Research Establishment
Building H36
Aldermaston, Reading RG 7 4PR
United Kingdom

Attn: J. C. Martin   1 copy